Reinforcement-concrete bond in discrete modeling of structural concrete

Gu, Dawei; Mustafa, Shozab; Pan, Jinlong; Lukovic, Mladena

DOI
10.1111/mice.12937

Publication date
2022

Document Version
Final published version

Published in
Computer-Aided Civil and Infrastructure Engineering

DOI: 10.1111/mice.12937

RESEARCH ARTICLE

COMPUTER-AIDED CIVIL AND INFRASTRUCTURE ENGINEERING WILEY

Reinforcement-concrete bond in discrete modeling of structural concrete

Dawei Gu[1,2] | **Shozab Mustafa**[1] | **Jinlong Pan**[2] | **Mladena Luković**[1]

[1]Concrete Structures, Faculty of Civil Engineering and Geosciences, Delft University of Technology, Delft, The Netherlands

[2]School of Civil Engineering, Southeast University, Nanjing, China

Correspondence
Mladena Luković, Concrete Structures, Faculty of Civil Engineering and Geosciences, Delft University of Technology, 2628 CN, Delft, The Netherlands.
Email: M.Lukovic@tudelft.nl

Funding information
Dutch Organization for Scientific Research (NWO) under the grant "Optimization of interface behaviour for innovative hybrid concrete structures" (Project Number: 16814); Key Project of National Natural Science Foundation of China (project number: 52130210)

Abstract

The bond between concrete and reinforcement is one of the critical parameters influencing the structural behavior of reinforced concrete (RC). This research proposes a mathematical methodology to scale the reinforcement-concrete bond-slip relationship in a beam lattice modeling framework. A simplified, generalized approach based on stochastic analysis is proposed to model the interaction between the reinforcing bar and surrounding concrete at the macroscale. The approach considers the randomness of the lattice mesh and the mesh size and adopts an analytical model for the interface assuming the pull-out failure of reinforcement as input, thereby including also the mesoscale geometric effect of ribs. By using the geometric configuration of Delaunay triangulation in the random lattice mesh, the interface elements can reproduce the basic conical stress transfer mechanism in concrete. Consequently, depending on boundary conditions, and without changing the interface properties, a splitting failure and bond-slip relation for splitting failure can be predicted. The model is systematically validated in different types of pull-out tests, through flexural and finally shear tests. With limited input (properties of the concrete and analytical equation for pull-out failure), having a (strong) physical background, the model was shown to capture the fundamental fracture mechanisms in RC under different loading and confinement conditions.

1 | INTRODUCTION

The bond property between reinforcement and concrete significantly influences the structural behavior of reinforced concrete (RC) members, including the load-carrying capacity, crack propagation, deformational capacity, and seismic resistance. Therefore, it is important to adopt appropriate reinforcement-concrete interface properties when simulating the mechanical behavior of RC structures. Still, the reinforcement-concrete bond behavior is complicated since it depends on many configuration details, for example, cover thickness, reinforcement geometry and diameter, reinforcement rib spacing, stress state of the reinforcement, confinement conditions, and the concrete strength. Furthermore, the evaluation of bond resistance is complex since different failure modes can develop (i.e., the reinforcement being pulled out or concrete splitting with a number of failure sub-modes depending on section geometry) and the influence of each parameter varies widely. To study the bond transfer

mechanism, a set of experimental work has been conducted (Bado et al., 2021; Goto, 1971; Gribniak et al., 2020). It is widely accepted that the bond between reinforcement and concrete can be attributed to the adhesion, friction, and concrete interlocking between ribs. Premature concrete splitting failure can happen prior to reinforcement pull-out if the confinement from surrounding concrete or transverse reinforcement is deficient. To quantify the bond stress-slip relationship under various boundary conditions, numerous analytical models have been established (Eligehausen et al., 1982; Ferguson, 1966; Mirza & Houde, 1979). In particular, based on extensive experimental data, Harajli et al. (1995, 2004, 2009) proposed a bond stress–slip model for rebars in normal concrete, fiber-RC (FRC) and concrete confined by fiber reinforced polymer under monotonic and cyclic loading. This analytical model considers a wide range of factors, including the loading and confinement condition, rib spacing of rebar, type of concrete, and other factors affecting bond behavior.

When simulating the structural behavior of RC using the finite element method (FEM), the bond element properties are related to the reinforcement diameter, cover thickness, and some other factors that are experimentally difficult to control, such as lateral pressure from confinement, boundary conditions, and stress state in the considered test setup. Meanwhile, it should be noted that the stress state of the concrete near the reinforcement is fictitious and cannot be validated since the interaction between reinforcement ribs and the surrounding concrete cannot be accurately evaluated. To overcome these uncertainties and represent the bond and boundary conditions as detailed as possible, researchers (Cai et al., 2020; Kurumutani et al., 2017) model the reinforcement with rebar ribs at mesoscale using fine mesh discretization. In mesoscopic analysis, the ribs of the deformed bar can be well-represented by solid elements, treating the shear transfer mechanism as the local contact between ribs and concrete in the neighborhood. Nevertheless, the huge computational cost due to fine mesh makes it impractical for analyzing the mechanical behavior of RC structures at macroscale. In past years, significant achievements have been made in the smeared-cracking models to simulate the cracking behavior of RC (Cervenka et al., 2022; Rimkus et al., 2020). However, these numerical models assume the concrete as a homogeneous material without imperfections and randomness, so usually they do not reflect the fracture features related to the material heterogeneity.

Compared to FEM, the discrete lattice model shows advantages in terms of concrete fracture analysis, especially in modeling the crack propagation (Qian, 2012; Schlangen & Garboczi, 1997). With irregular meshing methodology, it can intrinsically represent the heterogeneity of concrete and the material nonlinearity under various loading conditions. Therefore, the discrete lattice model has been widely applied in studying the fracture mechanism of concrete at the micro- and mesoscale (Bolander & Sukumar, 2005; Fascetti et al., 2022; Luković et al., 2015). Only recently studies using a lattice model to simulate the structural behavior of RC at the macroscale have been reported (Alnaggar et al., 2019; Pan et al., 2017; Sasano et al., 2018), where one of the main challenges is modeling the reinforcement-concrete interface. The researchers have also modeled the ribbed shape of deformed steel bars with fine mesh with explicit modeling of the fundamental interaction between ribs and surrounding concrete (Avadh et al., 2022; Karam et al., 2019; Šavija et al., 2013). However, when upscaling the lattice approach to the macroscopic structural behavior of RC members, the high computational cost limits its application.

Instead of modeling the three-dimensional (3D) ribbed shape of reinforcement in lattice modeling, some researchers attempted to simplify the procedure and treated the reinforcement as a one-dimensional beam or truss elements (Aydin et al., 2019; Bhaduri et al., 2021; Mustafa et al., 2022). In a discrete rigid body spring model (RBSM), the reinforcement beam elements are connected to concrete particles through zero-length linkage spring elements, for which the constitutive law can be defined by the local bond stress-slip relationship between reinforcement and concrete (Bolander et al., 2000; Gedik et al., 2011; Yip et al., 2005). Recently, Farooq et al. (2020, 2022) examined the validity of such a methodology by simulating two-end pull-out tests and beam bending with lap splices. In these simulations, the linkage spring elements were assigned with the bond stress-slip relationship of pull-out failure (instead of bond-splitting failure), which also takes into account the geometric properties of the reinforcement (i.e., ribs). This relationship was regarded as the inherent property of the reinforcement-concrete interface and parametrically independent. It was found that due to the unique geometrical features of irregular Voronoi mesh, the simplified reinforcement beam elements could reproduce a realistic conical cracking mechanism as observed in the tests. Moreover, the influence of cover thickness, reinforcement diameter and stirrup confinement on the bond stress-slip behavior could be well-predicted, which proved its feasibility in macroscopic mechanical analysis of RC structures.

Different from the RBSM, the Delft lattice model utilizes beam elements to represent all the phases, including concrete, reinforcement, and their interface (Luković et al., 2017). However, the interface element properties, so far, were determined by calibration of parameters such as the failure load, crack pattern, and crack propagation (Luković et al., 2017), or more recently crack widths in the experiments (Mustafa et al., 2022). This limits the use of the

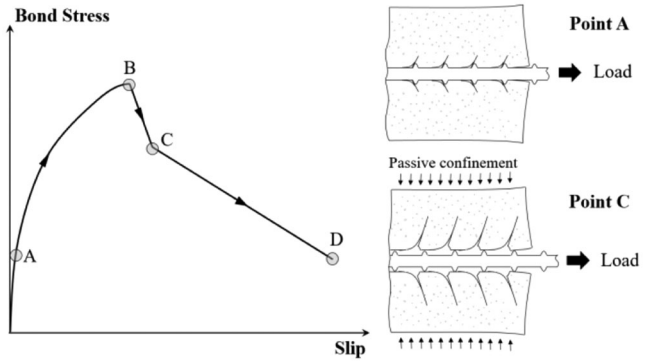

FIGURE 1 Typical bond stress-slip response for reinforcement in concrete

lattice model in structural analysis as the physical background of the reinforcement-concrete bond is missing and the predictive calculations cannot be made.

This research proposes a mathematical methodology to scale the constitutive parameters of the bond-slip relationships between concrete and reinforcing steel, in a beam lattice modeling framework. A simplified, generalized approach, based on stochastic analysis and with a small number of input parameters having a (strong) physical basis, is proposed to model the interaction between the reinforcing bar and surrounding concrete in a discrete-type random lattice model at the macroscale. In the model, concrete, reinforcement, and reinforcement-concrete interaction (interface) are all simulated as beam elements. A methodology for calculating the properties of the reinforcement-concrete interface element (strength and elastic modulus) is proposed based on the analytical relation of Harajli (2009) assuming the pull-out failure of reinforcement, and a stochastic analysis of mesh randomness. As a result, by using the relation for pull-out failure, being fully defined by reinforcement diameter, spacing of ribs and the strength of concrete, and with no additional input other than concrete properties (strength and elastic modulus), the behavior of possible splitting was predicted numerically, including the important and difficult to grasp the effect of confinement. To investigate the robustness of the model, varying boundary conditions and failure modes in pull-out tests are simulated. Furthermore, the approach is validated by simulating the structural behavior of RC members at the macroscale: in a flexural and a shear test.

2 | BOND-SLIP BEHAVIOR OF REINFORCEMENT IN CONCRETE: EXPERIMENTAL INSIGHTS AND ANALYTICAL FORMULATIONS

A typical bond stress-slip relation of the reinforcement in concrete is shown in Figure 1 along with the schematized bond-slip mechanism under splitting failure. In the initial loading stage, a small slip with a significant increase in bond stress is observed. During this early phase, the bonding is predominantly due to chemical adhesion accompanied by friction that is activated usually after adhesion failure. With a further increase in the slip, the radial component of rib bearing force causes splitting cracking of surrounding concrete, accompanied by a decrease in stiffness (Point A in Figure 1). When the residual tensile stress and passive confining stresses of surrounding concrete cannot further resist the increasing bearing force, the ultimate bond strength is reached (Point B in Figure 1). A further increase in slip causes a sudden decrease in bond stress and a new equilibrium is achieved (Point C in Figure 1). Finally, the ribs of the reinforcement tend to ride up the concrete keys, and the bond resistance degrades gradually, indicating the final failure of the reinforcement-concrete bond (Point D).

For reinforcement with effective confinement, for example, with dense transverse reinforcement, prestressing, or addition of fibers in the concrete matrix, a pull-out type of failure is observed instead of the aforementioned failure governed by the splitting of concrete. Under the confined situation, an increased bond strength and higher ductility are observed for the reinforcement-concrete interface. To represent the bond behavior of reinforcement in confined or unconfined concrete under monotonic loading, Harajli et al. (1995, 2004, 2009) proposed an analytical model as schematically shown in Figure 2.

In this monotonic envelope model, the bond stress-slip behavior for an ordinary splitting failure in two conditions (confined and unconfined—plain concrete) is divided into four stages: (1) following the pull-out failure envelope from zero until a bond stress of αu_{sp} (where $\alpha = 0.7$ and u_{sp} is the splitting bond strength, which is dependent on concrete compressive strength $f_c^{'}$, reinforcement diameter D, smallest concrete cover thickness c and stirrup confinement factor K_c); (2) when the stiffness changes and the bond stress increases almost linearly from αu_{sp} to the peak stress u_{sp}, with the corresponding slip displacement denoted as s_{sp}; (3) when the bond stress drops rapidly to u_p (for confined concrete) or βu_{sp} (for plain concrete), where $\beta = 0.65$ for normal strength concrete ($f_c^{'} \leq 48$MPa); and (4) finally, the bond stress progressively diminishes to zero. To represent a dominant pull-out failure instead of splitting, the behavior is also divided in four stages: (1) the bond stress increases from 0 to u_m at a corresponding slip of s_I, following the relationship $u = u_m(s/s_I)^{0.3}$, where u_m is only related to the concrete compressive strength $f_c^{'}$; (2) a ductile slipping plateau without bond stress loss until a slip of s_{II}; (3) a linear decrease in bond stress from the slip s_{II} to s_{III} until (4) when a constant residual bond stress u_f is reached, where $u_f = 0.35u_m$. Further details about all the parameters can be found in Harajli (2009).

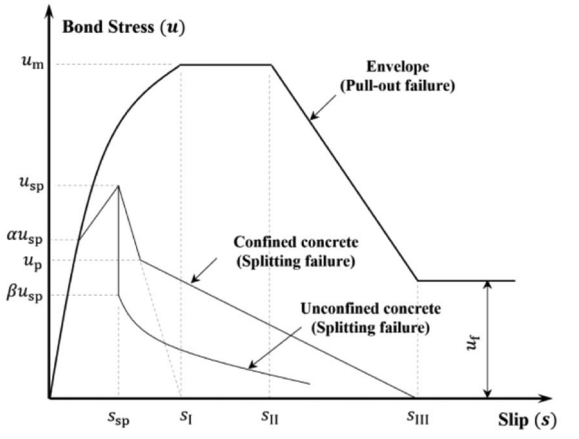

Expression of parameters
$\alpha = 0.7 \quad \beta = 0.65 \quad \gamma = 0.78$
$s_I = 0.15c_0$ (c_0 is clear distance between the ribs on bars)
$s_{II} = 0.35c_0$
$s_{III} = c_0$
$s_{sp} = s_I e^{3.3\ln(u_{sp}/u_m)} + s_0 \ln(u_m/u_{sp})$, For normal concrete
$s_{sp} = s_I e^{1.8\ln[(u_{sp}/u_m)^2 - 1]}$, For fiber-reinforced concrete
$u_m = 2.57\sqrt{f_c'}$ (f_c' is cylindrical concrete compression strength)
$u_{sp} = \gamma\sqrt{f_c'}\left(\frac{c + K_c}{D}\right)^{2/3} \le u_m$ (c is the smallest concrete cover thickness)
$u_p = u_{sp}(0.5 + K_{cs}),\ \beta u_{sp} \le u_p \le u_{sp}$
$u_f = 0.35u_m$ (K_c and K_{cs} are stirrup confinement factor)

FIGURE 2 Monotonic envelope model suggested by Harajli (2009)

This model considers many detailed parameters (e.g., c_0 is the clear distance between the ribs on bars; K_c and K_{cs} are the confinement factors, related to configuration details such as concrete cover thickness, stirrup spacing, etc.). That is why this model, accompanied by experimental insights, is further used for lattice modeling and validation of the numerical approach. Note that other empirical or analytical bond-slip models can also be used as this research is aimed at developing a procedure to translate the chosen bond-slip behavior to the properties of the reinforcement-concrete interface element.

3 | DISCRETE LATTICE MODEL

In the traditional lattice model (Schlangen & Garboczi, 1997), the continuum of interest is discretized into a set of beam elements that form a lattice mesh, and are assigned linear elastic properties, that is, Young's modulus and

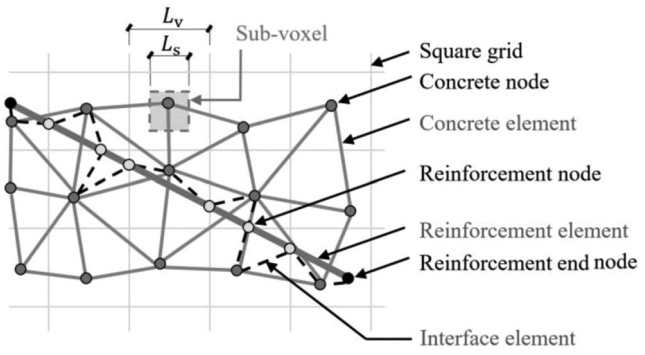

FIGURE 3 2D representation of the lattice mesh for reinforced concrete (RC)

tensile/compressive strength. The external load is then applied in steps to the lattice mesh. In each step, a linear elastic analysis is performed and the stress-to-strength ratio is calculated for all the elements. The element with the highest stress-to-strength ratio is then removed from the lattice mesh. It should be noted that although all phases are modeling by beam elements, only their axial stress and strength are considered when calculating the stress-to-strength ratio. After removing the critical element, the stresses in all the elements are released and the next loading step is applied. The analysis procedure is then repeated sequentially step by step until the pre-determined displacement or ultimate failure of the structure is reached.

Whereas originally the model is used for material research: for fracture analysis of conventional concrete (Schlangen & Garboczi, 1997) and recently for modeling time-dependent mechanical behavior of 3D printed concrete (Chang et al., 2021) and creep (Gan et al., 2021), in this research, the concept is further developed to simulate structural behavior of RC. To simulate the ductility of (some of) the lattice beam elements (like reinforcement), a non-linear stress-strain relation can be ascribed to these elements. In that case, during analysis, the element is not immediately removed from the mesh, but its properties are updated according to the assigned stress-strain relation. The detailed procedure for establishing the lattice mesh for RC is described below and is depicted in Figure 3.

Create grid: A cubical grid is made (square for two-dimensional [2D] mesh) with a certain voxel size of L_v, as labeled in Figure 3.

Generate concrete nodes and elements: In each voxel, a sub-voxel with size L_s is created. The concrete node is then generated randomly within the sub-voxel—this introduces some disorder in the lattice mesh to represent the heterogeneity of concrete. As a result, although the fracture law used for simulating concrete elements in the lattice mesh is elastic and purely brittle, the simulated response is quasi-brittle with softening. The model allows

also explicit consideration of the material structure of multiphase cementitious materials such as concrete, mortar or paste (Luković et al., 2015), resulting in increased fracture energy. It should be noted that the model also allowed considering softening at the lattice element level, which can be either obtained experimentally (Hordijk, 1993) or numerically from a parameter-passing multiscale modeling scheme (Qian, 2012). The ratio between the size of the sub-voxel and the voxel, L_s/L_v, is defined as the randomness of lattice mesh and is an important parameter for lattice simulations (Schlangen & Garboczi, 1997). The closest concrete nodes are then joined with each other based on the Delaunay triangulation (D. T. Lee & Schachter, 1980).

Generate reinforcement nodes and elements: The reinforcement is then modeled in the lattice mesh based on the reinforcement geometry. The ends of reinforcement are recognized as its end nodes, and a reinforcement node is generated at each point where the reinforcement crosses the voxel. Two adjacent reinforcement nodes are then connected to each other to form a reinforcement element.

Generate interface elements: Reinforcement nodes are connected to the concrete nodes in the corresponding voxels by interface elements.

After generating all the elements, they are assigned certain material properties. Subsequently, the boundary conditions and the loads are defined, and the analysis is performed.

4 | PROPERTIES OF REINFORCEMENT-CONCRETE INTERFACE ELEMENTS

The reinforcement-concrete interface elements in the lattice model can be simulated using two different approaches as depicted in Figure 4: (1) by modifying the coordinates of concrete and reinforcement nodes in the voxels containing reinforcement elements such that the interface elements are always aligned with reinforcement elements (Oliver-Leblond, 2013) as shown in Figure 4a; (2) by keeping the disorder of the concrete nodes such that the interface elements are generated based on the randomness of concrete nodes (Luković et al., 2017) as shown in Figure 4b. For concrete members with a relatively small amount of reinforcement, both methods can be suitable. However, for those members with a high reinforcement ratio (a large amount of closely spaced bars) or the fiber-matrix interfaces in fiber-reinforced cementitious composites, the first method is less suitable, as it would lead to too much modification of concrete nodes affecting significantly the random lattice mesh.

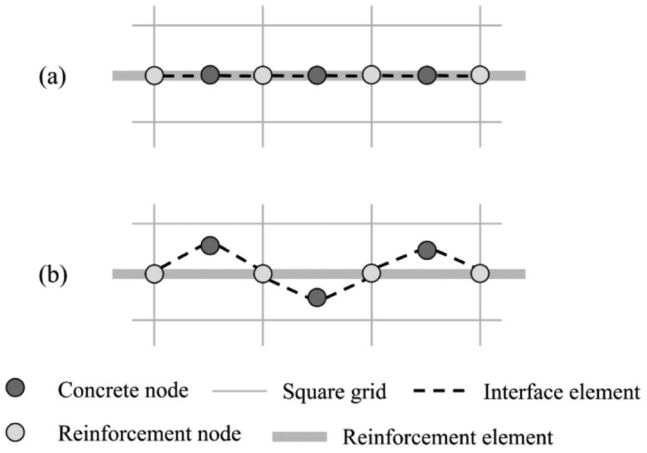

FIGURE 4 2D representation of reinforcement with (a) aligned and (b) non-aligned interface elements

Until now, for both approaches, the interface element properties are determined by inverse analysis such that crack patterns and crack widths correspond to experimental observations, with no physical background of the reinforcement-concrete bond parameters (Luković et al., 2017; Mustafa et al., 2022). In addition, with a second approach, a new calibration is needed once the randomness changes. In this study, a methodology for calculating reinforcement-concrete interface element properties, both for reinforcement with aligned and non-aligned interface elements, including different randomness of lattice mesh, is proposed based on the analytical reinforcement-concrete bond-slip model under pull-out failure suggested by Harajli (2009).

4.1 | Reinforcement with aligned interface elements

For reinforcement in concrete, the pull-out bond failure reflects the inherent property of the interface between reinforcement and the concrete matrix. Therefore, the envelope of the bond stress-slip curve from Figure 2 is utilized for determining the properties of interface elements in the lattice model. If the bond is strong enough to trigger a splitting failure, this failure should come out as a result of the model. Therefore, only parameters s_I, s_{II}, s_{III}, and u_m from Harajli's model are relevant for the suggested approach. Since the reinforcement-concrete interface exhibits a ductile behavior, the suggested bond stress-slip relationship is simulated using 15 segments, as shown in Figure 5, where the nth segment has a slip of s_n and bond stress of u_n. Note that more input segments can be defined in order to have more refined bond-slip relation but this results in higher computational cost.

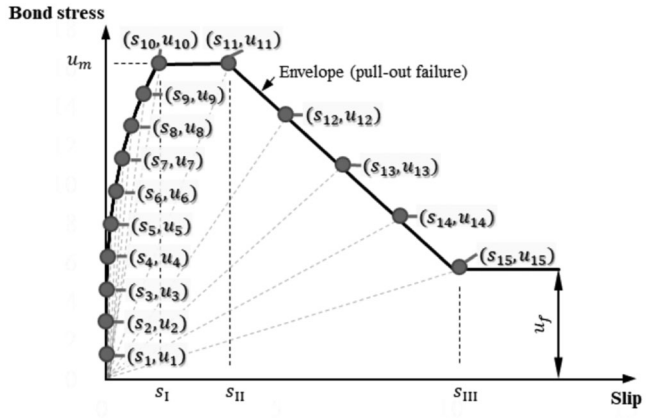

FIGURE 5 Definition of 15 segments for the input of bond stress-slip relationship in the lattice model

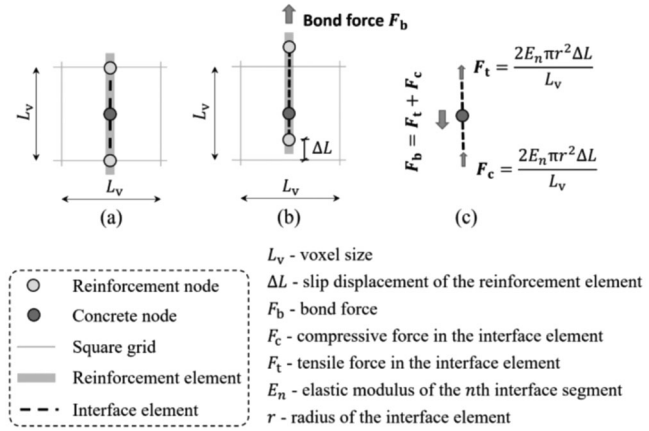

FIGURE 6 Schematic representation of the reinforcement slip for 2D aligned interface elements: (a) original state; (b) slipping; (c) equilibrium of free body

For each segment, a corresponding linear elastic stress-strain response of interface elements can be derived with the proposed procedure, including the elastic modulus E_n, tensile strength f_{tn} and compressive strength f_{cn}. When the tensile or compressive strength is reached during a certain loading step, the element properties are updated to $(n+1)$th segment, until the element breaks in the last segment, and then it is completely removed from the lattice mesh.

To determine the interface element properties, a single mesh grid with reinforcement aligned in y-direction and crossing through the center of the voxel is illustrated in Figure 6a. For the lattice mesh with grid size of L_v, a slip of ΔL aligned with the reinforcement element is assumed as shown in Figure 6b. For the interface element, the elastic modulus of the first segment E_1 is assumed to be the same as the concrete element E_c, that is $E_1 = E_c$. Then, the equilibrium of a free body for a matrix node with interface elements is established as illustrated in Figure 6c, all the notations can be found in the Appendix

Note that the value of the stiffness itself (elastic modulus, E_1) can take an arbitrary value because in a truss (or beam) model, the (axial) stiffness of the elements is considered, which also involves element radius (r). In the current lattice model, the radius of the lattice element is determined such that the effective elastic modulus of the whole lattice mesh is the same as that of the beam element. This is important as the chosen size of the radius would affect the ratio between bending and axial stiffness of the elements, which would cause different stresses among elements and would affect the fracture response (Lilliu, 2007).

Considering the equilibrium condition for the first segment, the expression for the radius of interface element r is obtained:

$$\frac{u_1}{s_1} = \frac{4E_1 r^2 \Delta L / DL_v^2}{\Delta L} \Leftrightarrow r = \sqrt{\frac{u_1 D}{E_c s_1}} \cdot \frac{L_v}{2} \tag{1}$$

where D is the diameter of the reinforcement. The tensile and compressive strengths of the interface element are assumed to be equal, and for the first segment are denoted by f_1. The pull-out stress acting over the circumference of the reinforcement u_1, has to be transferred by the reinforcement-concrete interface elements, having a strength f_1. When f_1 is reached, the equilibrium between internal force and bond load can be established:

$$\pi D L_v \cdot u_1 = 2\pi r^2 \cdot f_1 \Leftrightarrow f_1 = \frac{DL_v u_1}{2r^2} \tag{2}$$

For the nth segment of input, the elastic modulus E_n is determined by the stiffness of the interface element:

$$\frac{u_n}{s_n} = \frac{4E_n r^2 \Delta L / DL_v^2}{\Delta L} \Leftrightarrow E_n = \frac{u_n DL_v^2}{4 s_n r^2} \tag{3}$$

The shear modulus G_n is then calculated by:

$$G_n = \frac{E_n}{2(1+\nu)} \tag{4}$$

where ν is the Poisson's ratio of the interface element and is taken to be the same as that of the concrete matrix. By establishing a similar equilibrium as in Equation (2), the interface element strength for nth segment, f_n, is obtained:

$$f_n = \frac{DL_v u_n}{2r^2} \Leftrightarrow u_n = \frac{2 f_n r^2}{DL_v} \tag{5}$$

By transforming Equation (5), the bond strength u_n for reinforcement with aligned interface elements can be

represented by $2f_n r^2/DL_v$, which is denoted as $u_{n,\text{aligned}}$ in the subsequent derivations. The bond stiffness for nth segment K_n is defined as the bond force per unit slip distance, that is, $F_b/\Delta L$. Then, the bond stiffness of reinforcement with aligned interface elements $K_{n,\text{aligned}}$ can be obtained as

$$K_{n,\text{aligned}} = \frac{F_b}{\Delta L} = \frac{F_t + F_c}{\Delta L} = \frac{4E_n \cdot \pi r^2}{L_v} \tag{6}$$

It should be noticed that the aforementioned elastic modulus E_n and strength f_n are input material properties of interface elements in the lattice model, and the bond stiffness K_n and bond strength u_n are the structural properties of bond-slip relationship from Harajli's envelope (Harajli, 2009).

4.2 | Reinforcement with non-aligned interface elements

For the second approach, the concrete and reinforcement elements are not necessarily aligned. If the same input parameters derived for reinforcement with aligned interface elements are used for reinforcement with non-aligned interface elements, the output bond strength and stiffness can differ due to the randomness of the lattice mesh and the variation of element orientation. To quantify the influence of reinforcement position and also randomness of the lattice mesh on the output bond strength and stiffness, the 2D lattice mesh is considered first and then the procedure is extended to the 3D situation.

The X-Y plane of a 2D grid containing reinforcement and interface elements is presented in Figure 7a, and the coordinates of the concrete node are denoted by (x, y). The reinforcement is considered parallel to Y-axis in this case and the ends of the reinforcement element have coordinates $(m, 0.5L_v)$ and $(m, -0.5L_v)$, representing the two reinforcement nodes. When a nodal force is applied that activates the bond-slip behavior along positive y-direction (this force is further referred to as bond force F_b), there is a compressive force F_c and a tensile force F_t within the two interface elements as shown in Figure 7b,c. When the concrete node is located in the domain $[-0.5ran \cdot L_v \le x \le 0.5ran \cdot L_v, 0 \le y \le 0.5ran \cdot L_v]$, the interface compressive force F_c is larger than, or equal to the tensile force F_t, where ran is the specified randomness of the lattice mesh. When F_c reaches the interface strength ($F_c = f_n \cdot \pi r^2$), the compressed interface element fails.

To simplify the derivation, the following assumptions are made: (1) small deformation is assumed and the equilibrium of the free body is established on the undeformed structure, (2) only axial force and stiffness are considered for the interface beam elements, that is, they are regarded as truss elements. Note that the "truss element" assumption is made only for deriving the interface element properties, but in the lattice model analysis, all the elements are still regarded as beam elements. Considering the relatively small angle between interface and reinforcement elements, the axial force and stiffness of interface elements can govern their bending behavior, and the influence of these assumptions will be further validated in Section 5.1. According to the equilibrium of the free body in Figure 7, the bond force can be calculated as

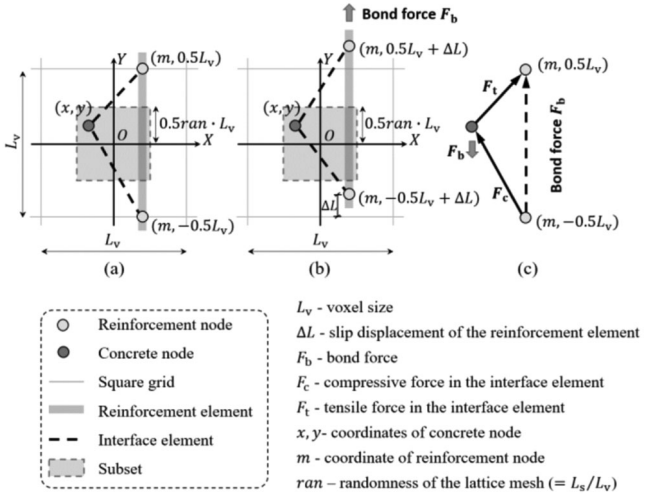

FIGURE 7 Schematic representation of the reinforcement slip for 2D non-aligned interface elements: (a) original state; (b) slipping; and (c) equilibrium of the free body

$$F_b = \frac{F_c L_v}{\sqrt{(x-m)^2 + (y + 0.5L_v)^2}} \tag{7}$$

where $F_c = f_n \cdot \pi r^2$. Then the maximum bond force is:

$$F_{b,\max} = \frac{\pi r^2 f_n L_v}{\sqrt{(x-m)^2 + (y + 0.5L_v)^2}} \tag{8}$$

Subsequently, the bond strength for reinforcement with non-aligned interface elements $u_{n,\text{non-aligned}}$ is calculated using

$$u_{n,\text{non-aligned}} = \frac{F_{b,\max}}{\pi D L_v} = \frac{r^2 f_n}{D\sqrt{(x-m)^2 + (y + 0.5L_v)^2}} \tag{9}$$

By incorporating the principle of virtual work, the bond-slip distance ΔL caused by F_b can be calculated as

$$\Delta L = \frac{F_b\left[(x-m)^2+(y-0.5L_v)^2\right]^{\frac{3}{2}}}{\pi r^2 E_n L_v^2} + \frac{F_b\left[(x-m)^2+(y+0.5L_v)^2\right]^{\frac{3}{2}}}{\pi r^2 E_n L_v^2} \quad (10)$$

Then, the bond stiffness for reinforcement with non-aligned interface elements $K_{n,\text{non-aligned}}$ is calculated as

$$K_{n,\text{non-aligned}} = \frac{F_b}{\Delta L} = \frac{\pi r^2 E_n L_v^2}{\left[(x-m)^2+(y-0.5L_v)^2\right]^{\frac{3}{2}}+\left[(x-m)^2+(y+0.5L_v)^2\right]^{\frac{3}{2}}} \quad (11)$$

Through Equations (6), (9), and (11), the ratio of bond strength, as well as bond stiffness between reinforcement with aligned and non-aligned interface elements, are calculated, assuming interface element strength as f_n:

$$\frac{u_{n,\text{non-aligned}}}{u_{n,\text{aligned}}} = \frac{L_v}{2\sqrt{(x-m)^2+(y+0.5L_v)^2}}$$

$$\frac{K_{n,\text{non-aligned}}}{K_{n,\text{aligned}}} = \frac{L_v^3}{4\left[(x-m)^2+(y-0.5L_v)^2\right]^{\frac{3}{2}}+4\left[(x-m)^2+(y+0.5L_v)^2\right]^{\frac{3}{2}}} \quad (12)$$

Since the concrete node is randomly located within the domain $[-0.5ran\cdot L_v \le x \le 0.5ran\cdot L_v, 0 \le y \le 0.5ran\cdot L_v]$, the expectation of the bond strength ratio and bond stiffness ratio is:

$$\mathrm{E}\left[\frac{u_{n,\text{non-aligned}}}{u_{n,\text{aligned}}}\right] = \int_0^{0.5ran\cdot L_v}\int_{-0.5ran\cdot L_v}^{0.5ran\cdot L_v} f(x)\cdot f(y)\cdot\frac{L_v}{2\sqrt{(x-m)^2+(y+0.5L_v)^2}}dxdy$$

$$\mathrm{E}\left[\frac{K_{n,\text{non-aligned}}}{K_{n,\text{aligned}}}\right] = \int_0^{0.5ran\cdot L_v}\int_{-0.5ran\cdot L_v}^{0.5ran\cdot L_v} f(x)\cdot f(y)\cdot\frac{L_v^3}{4[(x-m)^2+(y-0.5L_v)^2]^{\frac{3}{2}}+4[(x-m)^2+(y+0.5L_v)^2]^{\frac{3}{2}}}dxdy \quad (13)$$

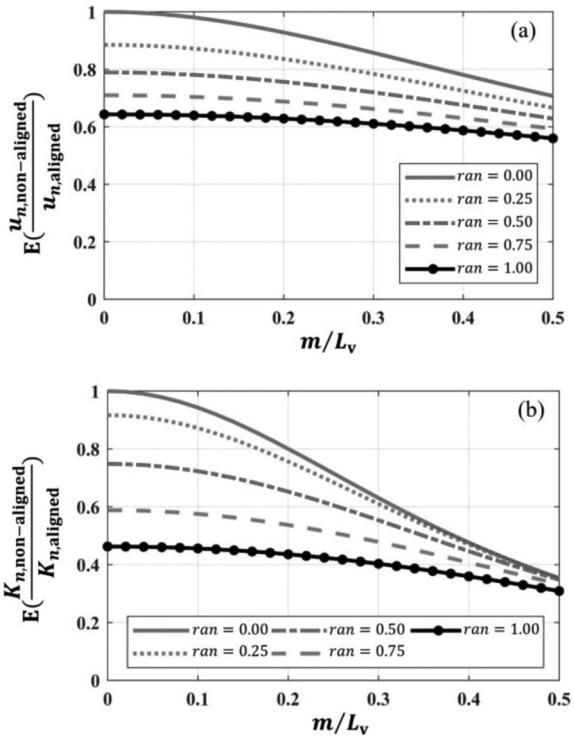

FIGURE 8 Relationship between the position of reinforcement, indicated by parameter m, and the expectation of (a) bond strength ratio and (b) bond stiffness ratio in a 2D lattice mesh, for different randomness of the lattice mesh

For the uniform distribution of concrete node coordinates, the probability density for x and y is:

$$f(x) = \frac{1}{ran\cdot L_v},\ -0.5ran\cdot L_v \le x \le 0.5ran\cdot L_v$$

$$f(y) = \frac{2}{ran\cdot L_v},\ 0 \le y \le 0.5ran\cdot L_v \quad (14)$$

By incorporating Equation (14) in Equation (13), the relationship between the expectation of bond strength and bond stiffness ratio and reinforcement position with various randomness is obtained and is shown in Figure 8. For the randomness of 0.5, the calculated bond strength ratio $\mathrm{E}[\frac{u_{n,\text{non-aligned}}}{u_{n,\text{aligned}}}]$, and bond stiffness ratio $\mathrm{E}[\frac{K_{n,\text{non-aligned}}}{K_{n,\text{aligned}}}]$, and corresponding reinforcement position m are also listed in Table 1.

When the concrete nodes are located within the domain $[-0.5ran\cdot L_v \le x \le 0.5ran\cdot L_v, -0.5ran\cdot L_v \le y \le 0]$, the interface compressive force (F_c) would be smaller than the tensile force (F_t), and the bond strength would be reached when F_t reaches the interface strength

TABLE 1 Calculated expectation of bond strength and bond stiffness ratio

$ran = 0.5$	$E[\frac{u_{n,non-aligned}}{u_{n,aligned}}]$		$E[\frac{K_{n,non-aligned}}{K_{n,aligned}}]$	
$m = n$	Two-dimensional (2D) mesh)	Three-dimensional (3D) mesh	2D mesh	3D mesh
0.0	78.9%	77.0%	74.9%	68.3%
$0.1L_v$	78.1%	75.4%	72.3%	63.9%
$0.2L_v$	75.7%	71.1%	65.2%	52.8%
$0.3L_v$	72.0%	65.2%	55.4%	39.5%
$0.4L_v$	67.6%	58.9%	44.7%	27.8%
$0.5L_v$	62.9%	52.8%	34.8%	19.1%

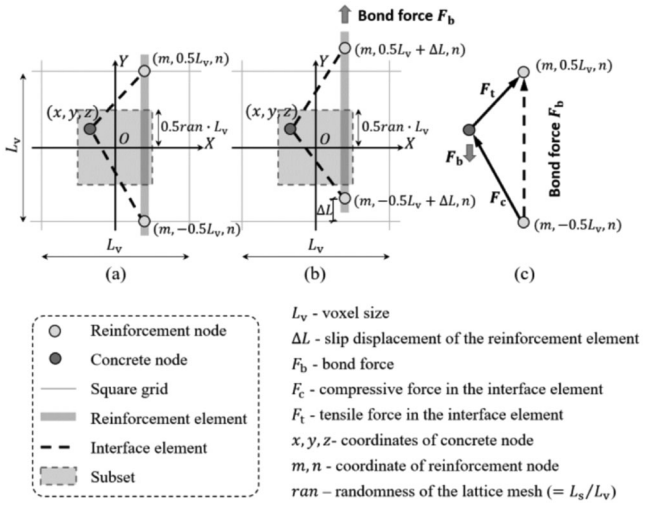

FIGURE 9 Schematic representation of the reinforcement slip for 3D non-aligned interface elements: (a) original state; (b) slipping; (c) equilibrium of free body

($F_t = f_n \cdot \pi r^2$). Similar derivation as for (F_c) is conducted and the same results are obtained which are shown in Figure 8.

For the 3D lattice mesh, a similar equilibrium of the free body is established as shown in Figure 9a–c. In this case, the coordinate of a concrete node is denoted by (x, y, z), and two ends of the reinforcement element have coordinates $(m, 0.5L_v, n)$ and $(m, -0.5L_v, n)$. The expectation of bond strength ratio and bond stiffness ratio is then expressed as shown in Equation (15):

$$\mathrm{E}\left[\frac{u_{n,\mathrm{non-aligned}}}{u_{n,\mathrm{aligned}}}\right] = \int_{-0.5ran\cdot L_v}^{0.5ran\cdot L_v}\int_{0}^{0.5ran\cdot L_v}\int_{-0.5ran\cdot L_v}^{0.5ran\cdot L_v} f(x)\cdot f(y)\cdot f(z) \cdot \frac{L_v}{2\sqrt{(x-m)^2+(y+0.5L_v)^2+(z-n)^2}}\,dxdydz$$

$$\mathrm{E}\left[\frac{K_{n,\mathrm{non-aligned}}}{K_{n,\mathrm{aligned}}}\right] = \int_{-0.5ran\cdot L_v}^{0.5ran\cdot L_v}\int_{0}^{0.5ran\cdot L_v}\int_{-0.5ran\cdot L_v}^{0.5ran\cdot L_v} f(x)\cdot f(y)\cdot f(z) \cdot \frac{L_v^3}{4[(x-m)^2+(y-0.5L_v)^2]^{\frac{3}{2}}+4[(x-m)^2+(y+0.5L_v)^2]^{\frac{3}{2}}}\,dxdydz \quad (15)$$

For the uniform distribution of concrete node coordinates, the probability density for x, y and z is:

$$f(x) = \frac{1}{ran\cdot L_v}, -0.5ran\cdot L_v \le x \le 0.5ran\cdot L_v$$

$$f(y) = \frac{2}{ran\cdot L_v}, 0 \le y \le 0.5ran\cdot L_v$$

$$f(z) = \frac{1}{ran\cdot L_v}, -0.5ran\cdot L_v \le z \le 0.5ran\cdot L_v \quad (16)$$

By combining Equations (15) and (16) and taking $m = n$, the relationship between the expected bond strength or stiffness ratio and reinforcement position with various randomness in the 3D mesh is derived (Figure 10). For the randomness of 0.5, the calculated $\mathrm{E}[\frac{u_{n,\mathrm{non-aligned}}}{u_{n,\mathrm{aligned}}}]$, $\mathrm{E}[\frac{K_{n,\mathrm{non-aligned}}}{K_{n,\mathrm{aligned}}}]$ and corresponding m and n are also listed in Table 1.

To obtain the bond strength of non-aligned interface elements the same as that of aligned ones, the strength and elastic modulus for non-aligned interface elements $f_{n,\mathrm{non-aligned}}$ and $E_{n,\mathrm{non-aligned}}$ are calculated with:

$$f_{n,\mathrm{non-aligned}} = \frac{f_{n,\mathrm{aligned}}}{\mathrm{E}[\frac{u_{n,\mathrm{non-aligned}}}{u_{n,\mathrm{aligned}}}]}$$

$$E_{n,\mathrm{non-aligned}} = \frac{E_{n,\mathrm{aligned}}}{\mathrm{E}\left[\frac{K_{n,\mathrm{non-aligned}}}{K_{n,\mathrm{aligned}}}\right]} \quad (17)$$

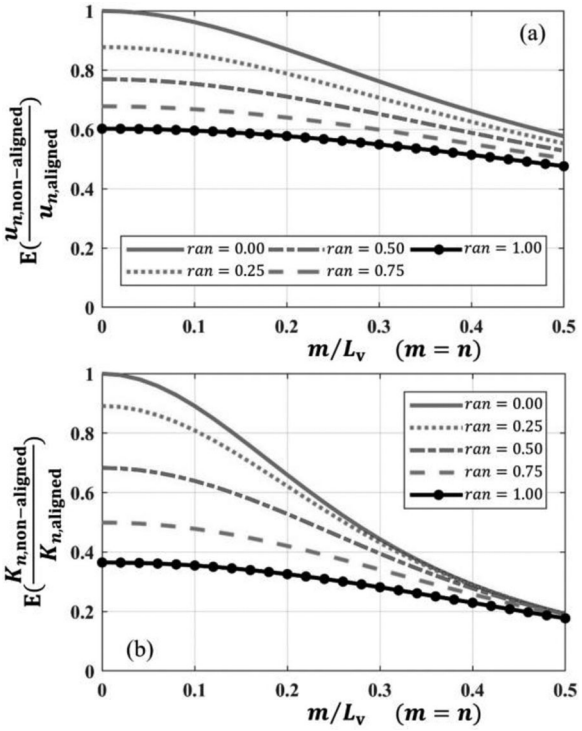

FIGURE 10 Relationship between the position of reinforcement, indicated by parameter m and n, and the expectation of (a) bond strength ratio and (b) bond stiffness ratio in a 3D lattice mesh, for different randomness of the lattice mesh

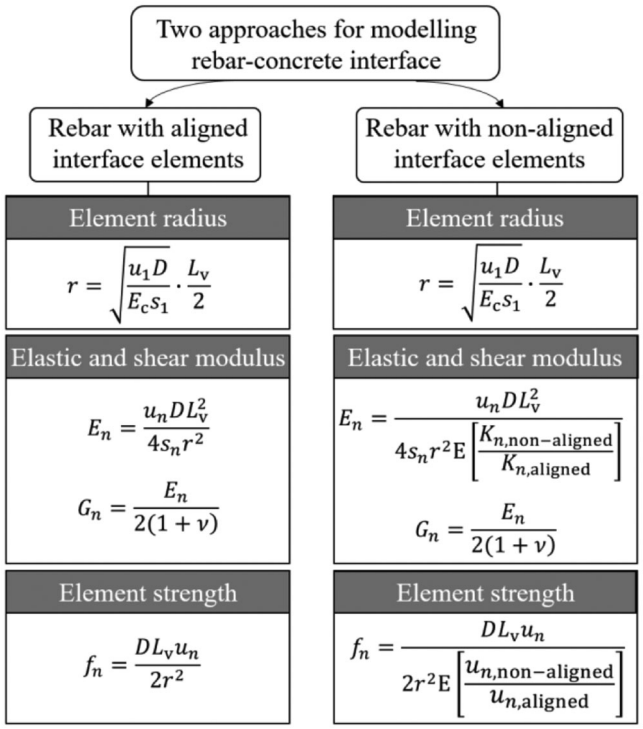

FIGURE 11 Generalized procedure for calculating the interface element properties for both aligned and non-aligned interface elements

where $f_{n,\text{aligned}}$ and $E_{n,\text{aligned}}$ represent the nth segmental element strength and elastic modulus of aligned interface elements. Figure 11 illustrates the generalized procedure for calculating the interface element properties for both aligned and non-aligned interface elements.

5 | VALIDATION OF THE PROPOSED METHOD FOR DETERMINING INTERFACE ELEMENT PROPERTIES

To validate the proposed approach for determining the reinforcement-concrete interface element properties, four different tests are simulated: one-end and two-end reinforcement pull-out tests and flexural and shear tests of the RC beam. For the flexural test, the bond between reinforcement and concrete would directly influence the crack width and crack spacing in concrete. For the shear test of the RC beam with shear reinforcement, higher interface bond strength enables more effective confinement of the shear cracks, resulting in higher shear carrying capacity (Regan & Kennedy Reid, 2004; Ye et al., 2018). Therefore, the appropriate modeling of the reinforcement-concrete bond is important in simulating both the flexural and shear behavior of RC structures, not only for the load-carrying capacity but also for the crack propagation, stresses in reinforcement, and the predicted failure mechanism.

5.1 | One-end pull-out test of reinforcement in concrete (pull-out failure)

The direct one-end reinforcement pull-out test, as designed by S. Lee et al. (2016), is simulated by a 3D lattice model. In this simulation, a reinforcement with a diameter of 12 mm is embedded in a concrete cube with a size of 180 mm (Figure 12). To prevent local cone failure of the matrix and induce a reinforcement-pull-out failure, the reinforcement is debonded over a certain length and

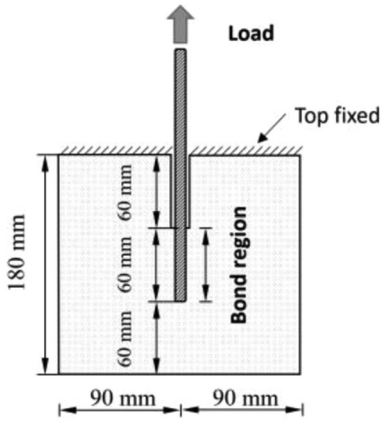

FIGURE 12 Details of embedded reinforcement and constraint condition for the one-end pull-out test of reinforcement in concrete

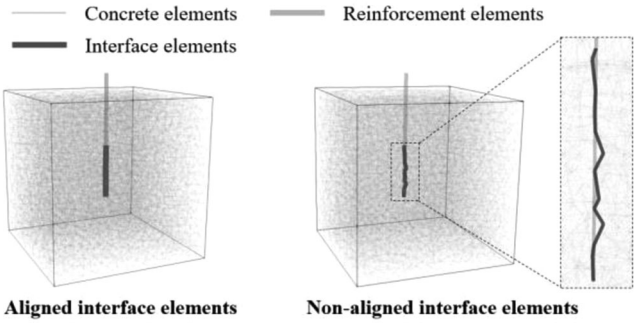

FIGURE 13 3D lattice meshes for reinforcement with aligned and non-aligned interface elements

the top surface of the concrete block is fixed. The embedment length of reinforcement is 60 mm (five times the reinforcement diameter). A tensile load is applied on the reinforcement end outside the concrete block. Under these boundary conditions, leading to reinforcement-pull-out failure, the inherent properties of interface elements can be examined.

Two 3D lattice meshes are simulated, one for reinforcement with aligned interface elements and the other for reinforcement with non-aligned interface elements as shown in Figure 13. When conducting the simulation, the analytical model proposed by Harajli (2009) is adopted to describe the pull-out behavior of reinforcement. The concrete strength class C30/37 is simulated, so compressive strength $f_c^{'}$, elastic modulus E_c, and Poisson's ratio are assumed to be 40 MPa, 34 Gpa, and 0.20, respectively. The steel reinforcement has a yielding strength f_y of 400 MPa, and the clear distance between ribs c_0 is 8 mm. The bond stress-slip relationship is subdivided into 15 segments. Each segment represents a linear-elastic behavior and has a bond strength u_n and corresponding slip distance s_n as listed in Table 2.

In simulations, a mesh size of 10 mm is adopted to validate the proposed methodology first, and then the same model with mesh size of 15 and 20 mm is conducted to study the mesh size effect. According to Equation (1), the radius of interface element r is calculated to be 5.1, 7.6, and 10.1 mm corresponding to the mesh size of 10, 15, 20 mm, respectively. For reinforcement with aligned interface elements, the elastic modulus E_n, shear modulus G_n, tensile strength f_{tn}, and compressive strength f_{cn} are calculated according to Equations (3) to (5) and listed in Table 2. For reinforcement with non-aligned interface elements, a concrete mesh randomness of 0.5 is adopted. The reinforcement is located along the center of the lattice mesh. According to Table 1, the expected bond strength ratio $E(\frac{u_{n,\text{non-aligned}}}{u_{n,\text{aligned}}})$ and bond stiffness ratio $E(\frac{K_{n,\text{non-aligned}}}{K_{n,\text{aligned}}})$ is calculated at 0.77 and 0.68, respectively. Then, the strength and elastic modulus of non-aligned interface elements can be obtained by Equation (17) as listed in Table 2. The comparison between the analytical model and the output of the simulation is shown in Figure 14.

For reinforcement with aligned interface elements, the simulation results fully fit the analytical model, which is

TABLE 2 Reinforcement-concrete interface parameters used as input in the lattice simulation for one-end reinforcement pull-out test (mesh size = 10 mm)

			Aligned interface elements (Input 1)				Non-aligned interface elements (Input 2)			
*n*th segment	s_n(mm)	u_n(MPa)	E_n(MPa)	G_n(MPa)	f_{tn}(MPa)	f_{cn}(MPa)	E_n(MPa)	G_n(MPa)	f_{tn} (MPa)	f_{cn} (MPa)
1	0.0006	1.63	34,000	14,167	3.79	−3.79	50,000	20,833	4.92	−4.92
2	0.0056	3.25	6746	2811	7.58	−7.58	9921	4134	9.84	−9.84
3	0.0217	4.88	2619	1091	11.36	−11.36	3852	1605	14.76	−14.76
4	0.0566	6.50	1339	558	15.15	−15.15	1969	820	19.68	−19.68
5	0.1191	8.13	795	331	18.94	−18.94	1170	487	24.59	−24.59
6	0.2186	9.75	520	217	22.73	−22.73	764	318	29.51	−29.51
7	0.3655	11.38	363	151	26.51	−26.51	533	222	34.43	−34.43
8	0.5704	13.00	266	111	30.30	−30.30	391	163	39.35	−39.35
9	0.8446	14.63	202	84	34.09	v34.09	297	124	44.27	−44.27
10	1.2000	16.25	158	66	37.88	−37.88	232	97	49.19	−49.19
11	2.8000	16.25	68	28	37.88	−37.88	99	41	49.19	−49.19
12	4.1000	13.61	39	16	31.72	−31.72	57	24	41.20	−41.20
13	5.4000	10.97	24	10	25.57	−25.57	35	15	33.20	−33.20
14	6.7000	8.33	14	6	19.41	−19.41	21	9	25.21	−25.21
15	8.0000	5.69	8	3	13.26	−13.26	12	5	17.22	−17.22

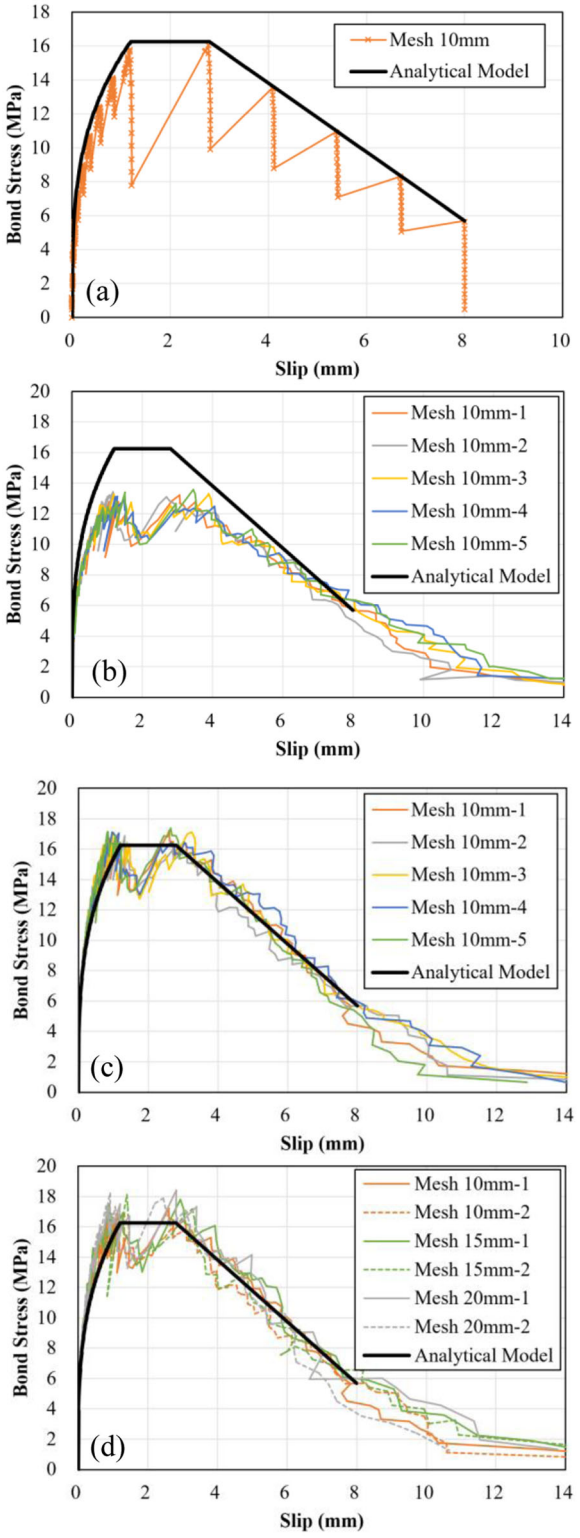

FIGURE 14 Bond stress-slip relationship by analytical model and simulation result: (a) aligned interface elements (Input 1 in Table 2); (b) non-aligned interface elements with unmodified input parameters (Input 1 in Table 2); (c) non-aligned interface elements with modified input parameters (Input 2 in Table 2); and (d) non-aligned interface elements with modified input parameters for different mesh sizes

used as input interface parameters as shown in Figure 14a. Note that the sharp decrease and increase between the slip 2 and 4 mm is due to a chosen number of segments, which are used to define the interface properties. Besides, the vertical drop of load derives from the element removal/update procedure used in the beam lattice approach, which can be mitigated by using an incremental calculating approach (Eliáš, 2015). For reinforcement with non-aligned interface elements, the voxels crossed by reinforcement are assigned with a randomness of 0.5. To validate the mesh discretization effect, the lattice model is re-meshed several times, and all simulation results are presented. If the same input element properties are used for both the aligned interface elements and non-aligned situations, a significant underestimation of the output bond strength is obtained as shown in Figure 14b. However, when using the input element properties modified according to the proposed method, the simulated bond stress-slip relationship matches the analytical model well as shown in Figure 14c. When modeling with different mesh sizes (10, 15, and 20 mm) as shown in Figure 14d, similar bond stress-slip responses are obtained since the derivation of interface properties considers the influence of mesh size. The damage pattern at a slip of 3.0 mm for simulated specimens is shown in Figure 15a–d. The final pull-out failure takes place due to the fracture of interface elements accompanied by some damage to the concrete elements. Both the aligned and non-aligned interface approaches can well represent the reinforcement-concrete bond-slip behavior. It should be pointed out that, apart from Harajli's analytical model (Harajli, 2009), any bond stress-slip law can be adopted, and the same approach can be used to determine interface element properties in different types of simulated materials/structures (e.g., in FRC, reinforced alkali-activated concrete).

5.2 | Two-end pull-out test of reinforcement in concrete (splitting failure)

When the confinement of reinforcement is not sufficient, splitting failure may happen instead of pull-out failure. To validate the proposed approach in modeling of the splitting bond behavior, the two-end pull-out experiments conducted by Iizuka et al. (2011) are simulated. In the experiments, the reinforcement was embedded in a 150-mm concrete cube at the desired concrete cover thickness and subjected to two-end pull-out load as shown in Figure 16. The average bond stress along the bond area was measured by the strain gauge attached on half-height of the reinforcement, and the slip of reinforcement was measured

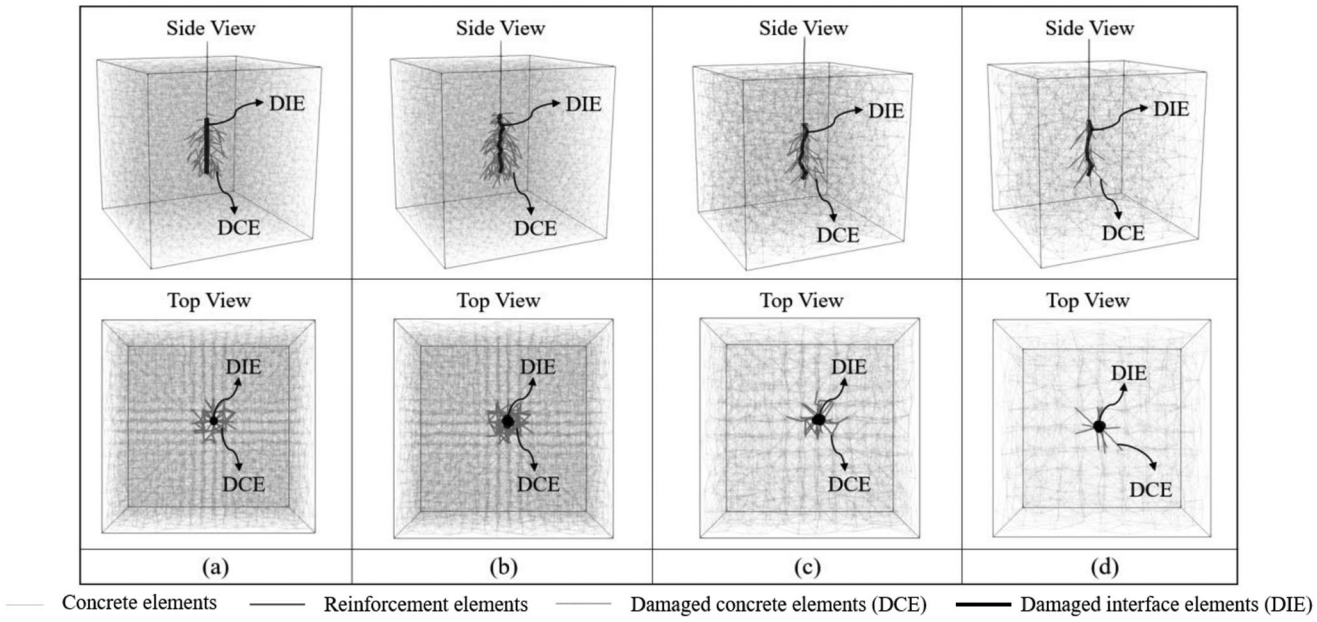

FIGURE 15 Damage pattern at a slip of 3.0 mm for one-end reinforcement pull-out: (a) aligned interface elements with mesh of 10 mm, Input 1; (b) non-aligned interface elements with mesh of 10 mm, Input 2; (c) non-aligned interface elements with mesh of 15 mm; and (d) non-aligned interface elements with mesh of 20 mm

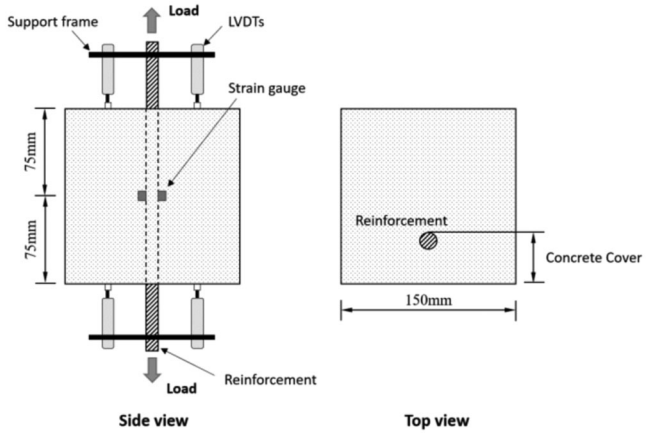

FIGURE 16 Details of embedded reinforcement for two-end pull-out test of reinforcement in concrete (Iizuka et al., 2011). LVDTs, linear variable displacement transducers

by a group of linear variable displacement transducers (LVDTs) at the top and bottom surface of the concrete cube.

Three specimens with cover thicknesses of 50, 30, and 10 mm are simulated to evaluate the influence of concrete cover thickness on bond stress-slip behavior. The concrete compressive strength is 28.3 MPa, and the rebar has a diameter of 19.1 mm and yielding strength of 1039 MPa. The 3D lattice model is established with the mesh size of 10 mm and randomly distributed non-aligned interface elements are simulated according to the proposed approach. Figure 17a–c shows the simulated bond stress-slip relationship for all three types of cover thickness, compared to experimental results. Note that in all three simulations, the same input for the rebar-concrete interface is defined.

In general, the lattice model matches the experimentally obtained bond-stress slip curve well, especially concrete covers 30 and 10 mm and for predicting the ultimate bond stress. In the experiment, an unusual stiffness decrease took place in the initial loading stage of the 50-mm concrete cover specimen. The authors (Iizuka et al., 2011) attributed this to the slip-detecting error, which explains the difference between the simulated and tested results for this specimen. Note that the light gray lines represent the linear analysis steps of the lattice model. At the endpoints of these lines, one element (either concrete, interface, or steel) reaches its strength and is removed. Subsequently, a new linear elastic analysis is performed. The characteristic zig-zag pattern (light gray lines) can be overcome by applying smoothening techniques so that an envelope is made. Only steps at the envelope are used in the analysis.

Figure 18 shows the simulated crack patterns chosen at different slip values for reinforcement with various concrete cover thicknesses. Different from the one-end pull-out test, in which the concrete top surface is constrained to form a strong confinement, the two-end pull-out test allows the formation of a conical cracking surface in concrete, similarly as experimentally observed (Farooq et al., 2022; Goto, 1971). A splitting failure happens instead of reinforcement pull-out, and the bond strength is reached due to the fracture of surrounding concrete, with the interface elements not reaching their peak strength. With the increasing slip, the cracks prop-

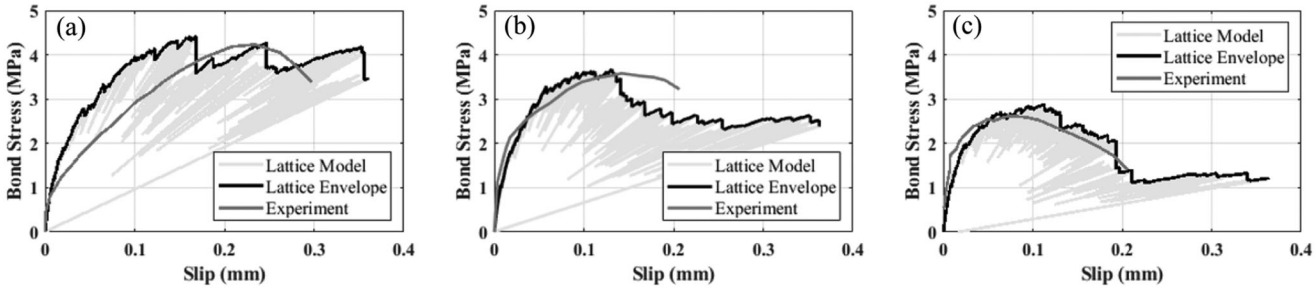

FIGURE 17 Tested and simulated bond stress-slip relationship for two-end pull-out tests of reinforcement with various concrete cover thickness: (a) concrete cover of 50 mm; (b) concrete cover of 30 mm; and (c) concrete cover of 10 mm

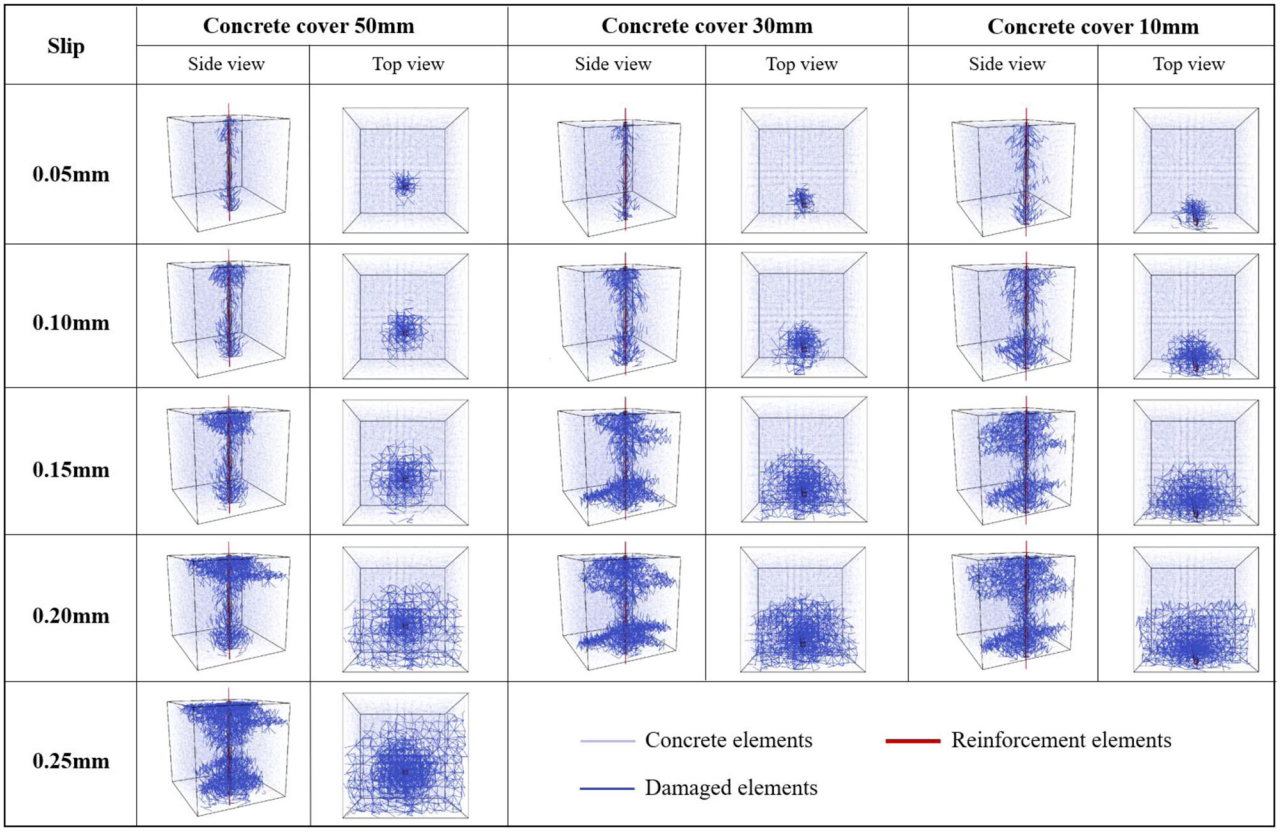

FIGURE 18 Simulated crack pattern under different slip for reinforcement with various concrete cover thickness

agate from the reinforcement-free end to its half-height and spread from the reinforcement center to the outside. At a slip of 0.05 mm, the cracks in the specimen with the thinnest concrete cover of 10 mm first reach the concrete edge, signifying the formation of longitudinal splitting cracks along reinforcement. With further deformation, a cone-shape cracking area forms in all the concrete blocks. When reducing the concrete cover thickness, the measured bond strength decreases although the same interface element properties are adopted for all three specimens. The splitting failure can happen due to the damage of the surrounding concrete before the interface elements reach their strength. With a smaller concrete cover thickness, the conical stress transferring area will be reduced, which means that the bond stress cannot be sufficiently transferred from the reinforcement surface to the surrounding concrete. Therefore, a downtrend in bond strength is found when reducing the concrete cover thickness.

Although a simplified interface element is used without modeling the 3D shape of ribs along a deformed bar, the fundamental conical stress transferring mechanism due to crack propagation from the rib surface can be

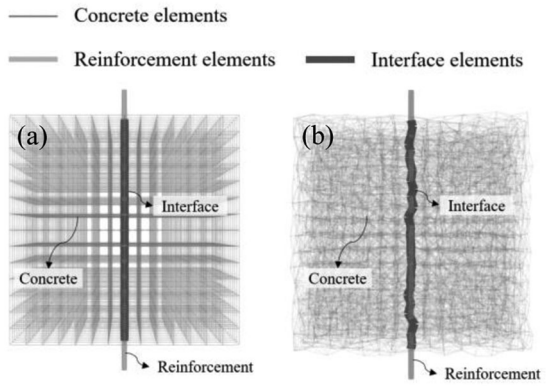

FIGURE 19 Side view of (a) quadratic mesh and (b) triangular mesh

well-simulated (Figure 18). To explore the mechanism behind it, the same two-end pull-out test is simulated using a regular quadratic mesh as shown in Figure 19a. The lattice mesh that was generated based on Delaunay triangulation (D. T. Lee & Schachter, 1980) is also shown in Figure 19b for comparison.

Figure 20a–c shows the simulated bond stress-slip relationship and crack pattern at peak load for the regular quadratic mesh. For all the specimens with different concrete cover thickness, no cone-shape cracking area is formed until ultimate failure, which means the conical stress transferring mechanism disappears by modifying the geometric shape of the mesh. It reveals that when the regular quadratic mesh is used, the bond stress cannot be sufficiently transferred to surrounding concrete but localizes in the vicinity of reinforcement. In the RBSM approach, the same phenomenon was found when representing the reinforcement-concrete interface by simplified spring linkage elements (Farooq et al., 2020, 2022).

Figure 21a illustrates a schematic diagram for concrete deformation and cracking following Goto's experimental observations (Goto, 1971) as well as the stress transfer mechanism in the triangular mesh (Figure 21b) and regular quadratic mesh (Figure 21c). In the experiments, the radial component of rib bearing force can cause splitting cracking of surrounding concrete at an angle of 45–60°. In the triangular mesh, the shear stress can transfer along the similar orientation, which represents the realistic cracking mechanism. Therefore, the discrete lattice mesh based on Delaunay triangulation has an inherent ability to reproduce the confinement effect on bond behavior, while the reinforcement-concrete interface properties do not need to consider the structural parameters like FEM does.

5.3 | Flexural behavior of the RC beam

To further validate the proposed approach in simulating full-scale structures, a four-point bending test for an RC beam failing in flexure is simulated. The details of the experimental setup are shown in Figure 22. During the experiment, LVDTs were used to measure the mid-span deflection. Besides, digital image correlation (DIC), which is a non-contact optical technique that allows the visualization of deformations and strain as full-field contour maps, was used. The measurements from DIC were limited to the constant moment region (central 500 mm of the beam) to

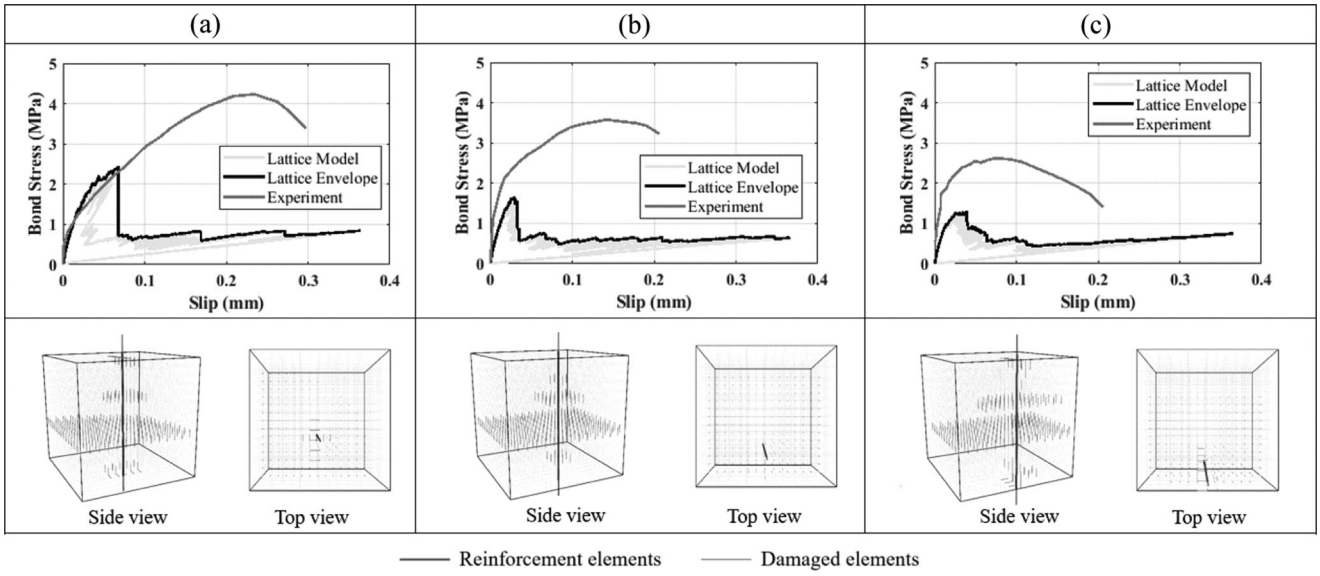

FIGURE 20 Simulated bond stress-slip relationship and crack pattern at peak load for the quadratic mesh: (a) concrete cover of 50 mm; (b) concrete cover of 30 mm; and (c) concrete cover of 10 mm

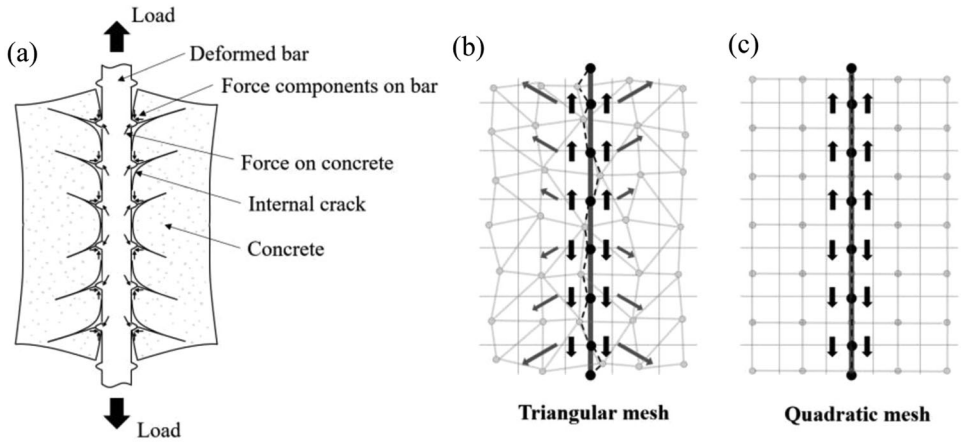

FIGURE 21 Schematic diagram for bond stress transfer mechanism of reinforcement in concrete: (a) internal cracks around the deformed bar and stress transfer mechanism based on the (b) triangular mesh, and (c) regular quadratic mesh

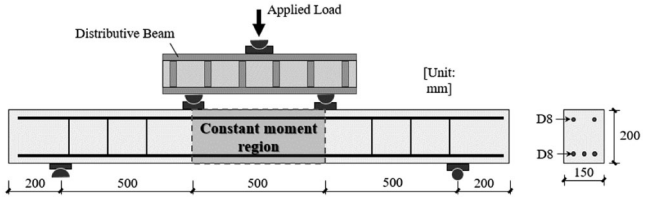

FIGURE 22 Schematic representation of flexural test setup with cross-sectional details

study the development of cracks under pure bending loads. Under these boundary conditions, the number, spacing, and width of cracks in the constant moment region are directly governed by the properties of the reinforcement-concrete interface. The compressive strength of concrete, measured on 100 mm cubes, was 49.4 ± 2.2 MPa, whereas steel B500 with a diameter of 8 mm and elastic modulus of 200 GPa was used as reinforcement.

For the simulation of the flexural beam, a mesh size of 10 mm is adopted. The input tensile and compressive strength of the lattice mesh are adjusted such that simulated strengths are equal to experimentally measured compressive strength of concrete and corresponding (calculated by Eurocode analytical formulations) tensile strength (CEN, 2004). The concrete elements are simulated using only one segment (brittle elements), while the reinforcement is simulated using 19 segments so that the appropriate ductility is captured in the model. For the reinforcement-concrete interface, 15 segments are used as shown in Figure 5.

In Figure 23a,b, respectively, the load-deflection response of the beam obtained experimentally and the development of the maximum crack width is compared with the simulated results. The maximum crack width in the experiment is determined using DIC. The experimental and numerical crack pattern of the beam during the

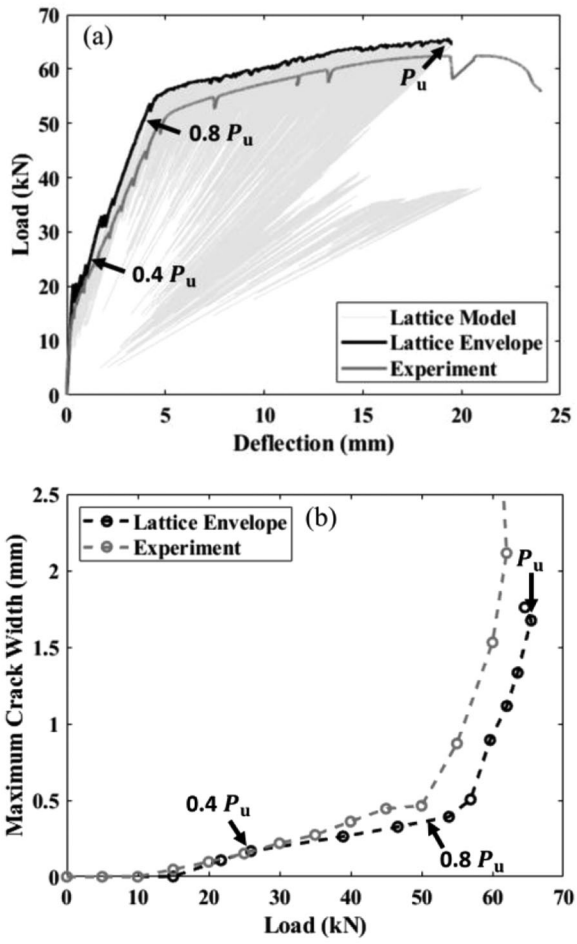

FIGURE 23 Simulated and experimental results for the flexural test of RC beam: (a) load-deflection; (b) load-maximum crack width

fracture process, including the stress distribution in the reinforcement at the peak load, are also shown (Figure 24).

The simulated results match the experiments well in terms of failure mode, peak load, and the deformation and

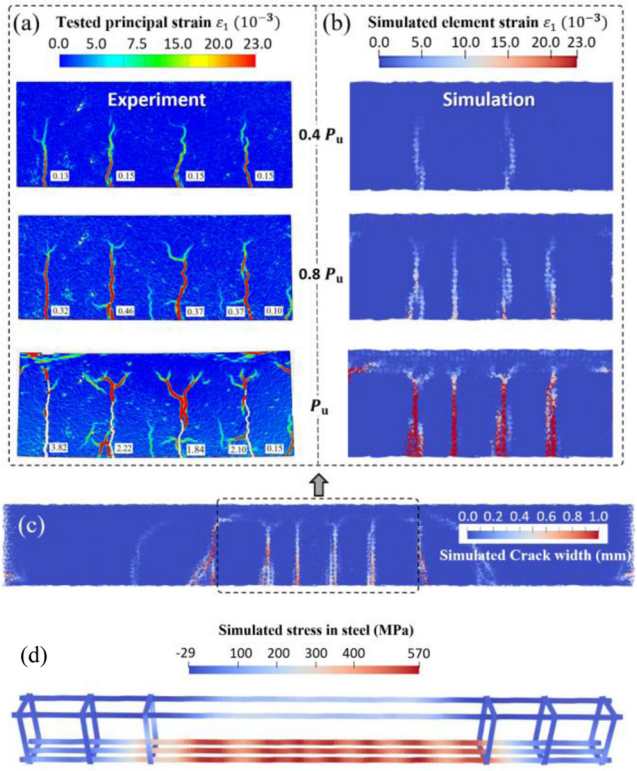

FIGURE 24 Crack patterns and steel stress of RC beam under flexural failure: (a) tested principal strain at the selected loads; (b) simulated element strain at the selected loads; (c) simulated crack width at the peak load; and (d) simulated stress of reinforcement at the peak load (P_u stands for the peak load)

crack spacing. Still, somewhat higher stiffness (Figure 23a) and smaller crack widths at the same load (Figure 23b) can be observed in the numerical results. Also, some differences can be observed in how the damage develops, showing that the stabilized cracking stage in the simulation is reached at higher load levels. Still, the simulation gives good predictions for the final crack pattern, load displacement curve, and crack width development, especially before yielding of the steel. The prediction error in terms of maximum load and corresponding crack width is about 5% and 10%, respectively. This validates the proposed reinforcement-concrete interface modeling approach for indicated boundary conditions.

5.4 | Shear behavior of RC beam

Shear behavior of the RC beam, as one of the most challenging failure mechanisms, is also tested and simulated. The details of the beam and test setup are shown in Figure 25. To measure the strain distribution along reinforcement and to enable detailed analysis and comparison with numerical results, a special continuous strain mea-

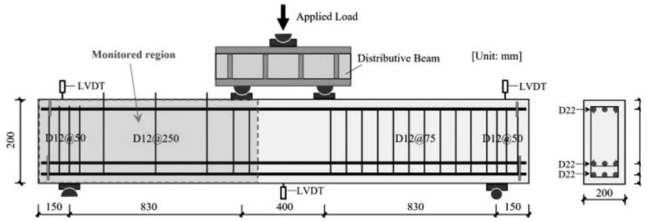

FIGURE 25 Schematic representation of shear test setup with cross-sectional details

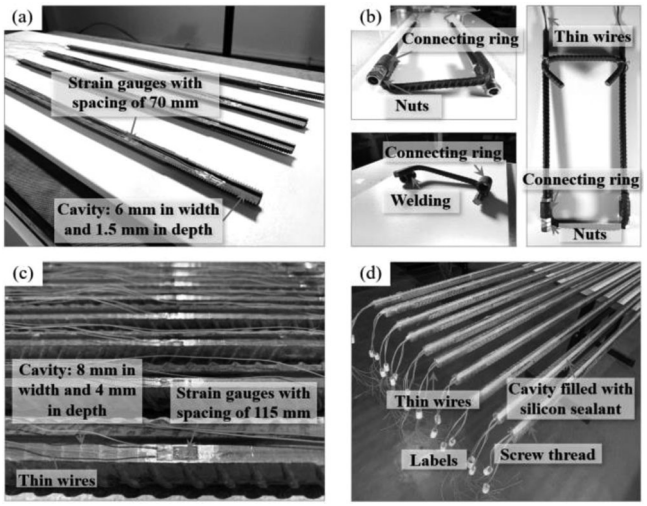

FIGURE 26 Fabrication of strain gauges: (a) cutting stirrup leg into two halves and making inside cavity; (b) assembling stirrups by high strength epoxy resin and nuts; (c) making cavity on longitudinal reinforcement surface; and (d) filling the cavity by silicon sealant (Gu et al., 2022)

suring methodology is adopted. The 3×6 mm cavity is made inside the stirrup legs and the 4×8 mm cavity is cut along the surface of longitudinal reinforcement. Then, a set of strain gauges are continuously attached to the cavity as shown in Figure 26. More details about the strain gauging system can be found in Gu et al. (2022).

To reduce the cost, only one span of the beam was designed with the continuous strain measuring system, and DIC was used to detect the full-field strain in concrete. The right span was strengthened with dense stirrups to prevent its shear failure. Along with the beam tests, cylinders with a diameter of 100 mm and a height of 200 mm were tested to determine the compressive strength and elastic modulus of concrete, which were 53.0 MPa and 36.1 GPa, respectively. The mean yielding strength of stirrups (with a diameter of 12 mm) was 440 MPa and of the longitudinal reinforcement (with a diameter of 22 mm) was 635 MPa. All reinforcement has an elastic modulus of 200 GPa.

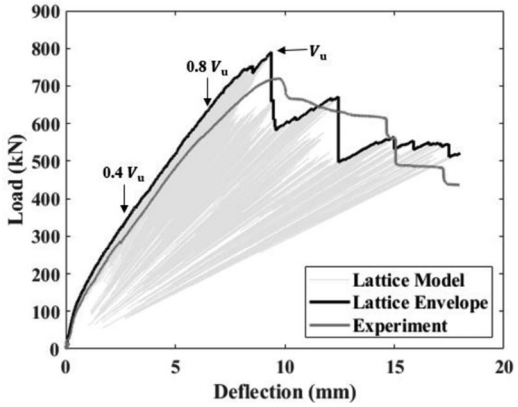

FIGURE 27 Load-deflection behavior for shear test of RC beam (V_u stands for the peak load)

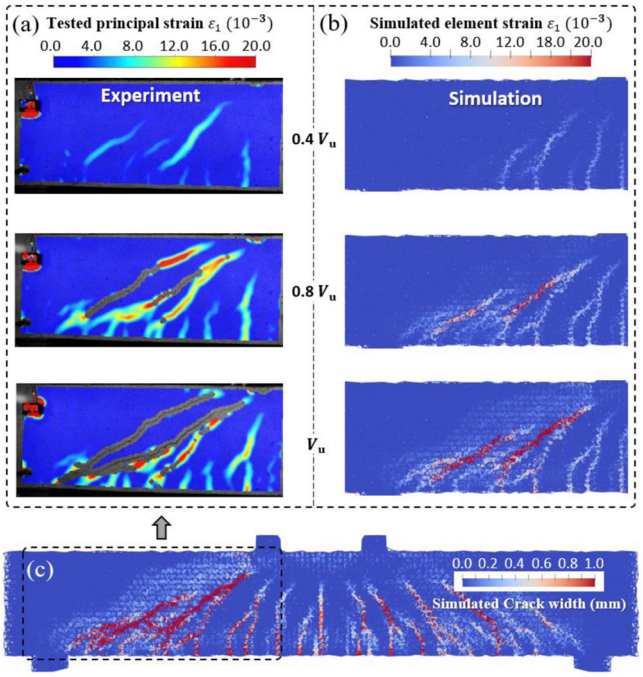

FIGURE 28 Crack patterns of the RC beam under shear failure: (a) tested principal strain at the selected loads; (b) simulated element strain at the selected loads; and (c) simulated crack width at the peak load (V_u stands for the peak load)

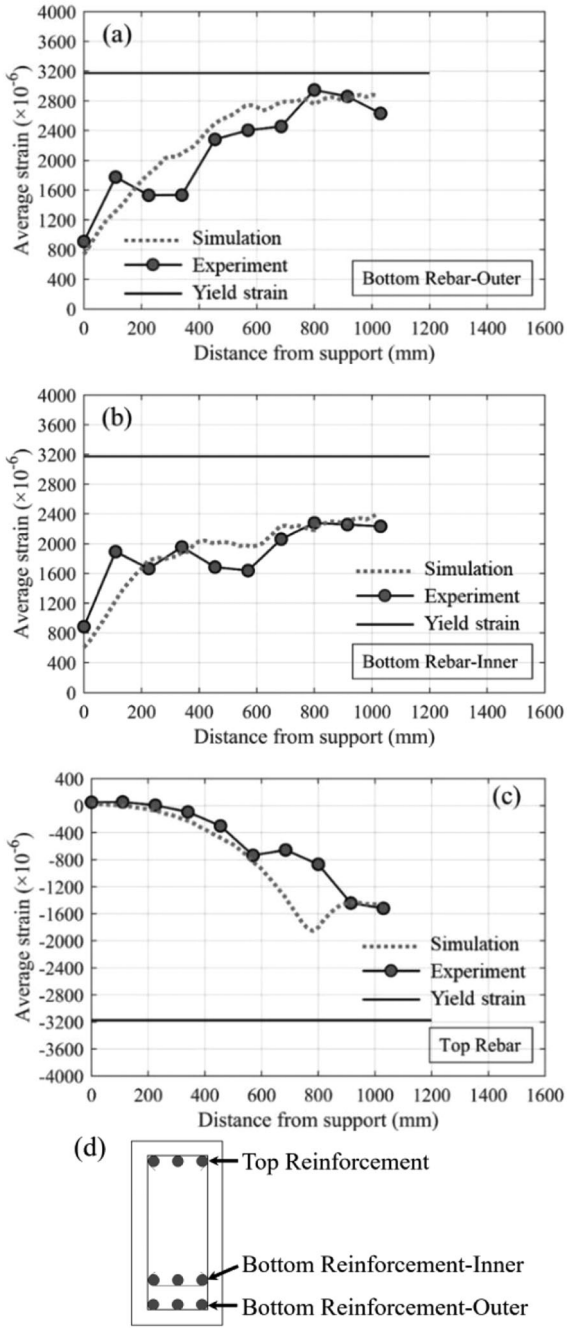

FIGURE 29 Strain distribution along longitudinal reinforcement at the peak load: (a) bottom reinforcement at outer layer; (b) bottom reinforcement at inner layer; (c) top reinforcement; and (d) schematic representation of reinforcement position

When simulating the shear behavior of the RC beam, due to the relatively large size of the beam, a coarser mesh size of 20 mm is used. The steel reinforcement is simulated using 19 segments and the reinforcement-concrete interface element properties are determined by the proposed approach, using 15 segments (Figure 5). The simulated load-deflection curve, crack growth due increasing load, and crack pattern at peak load are shown in Figures 27 and 28.

The numerical result matches the experimental results well in terms of load-deflection behavior, fracture development, and formation of critical shear cracks, and the prediction error in terms of shear carrying capacity is about 10%, whereas the numerical fracture pattern almost exactly matches the experimental one. In the simulation, the peak load is reached due to the compression failure of concrete elements near the loading plate, which is in line with the experimentally observed shear-compression failure.

Since the continuous strain-gauging system of reinforcement is utilized in the experiment, the measured strain

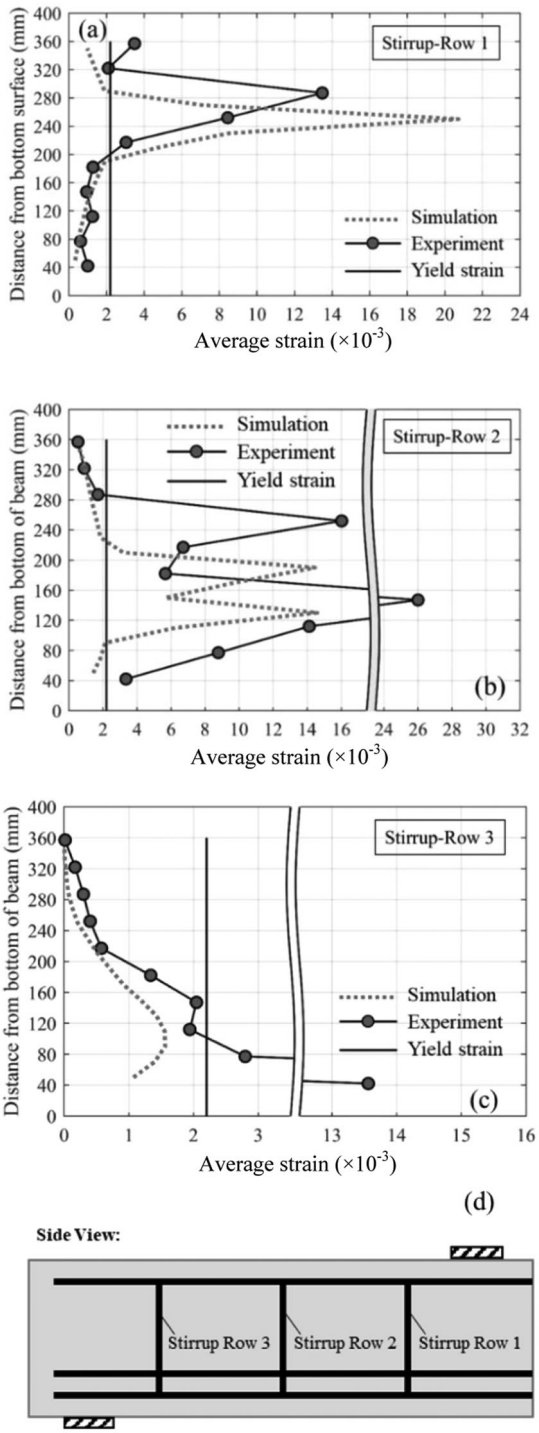

FIGURE 30 Strain distribution along stirrups at the peak load: (a) first row; (b) second row; (c) third row; and (d) schematic representation of reinforcement position

distribution along reinforcement can be directly compared with the simulated results. The average strain distribution along longitudinal and shear reinforcement at the peak load is shown in Figures 29 and 30, respectively.

Simulated results show the same trend and correspond well to the experimental results. Note that both in the experiment and simulation, the strain distribution along

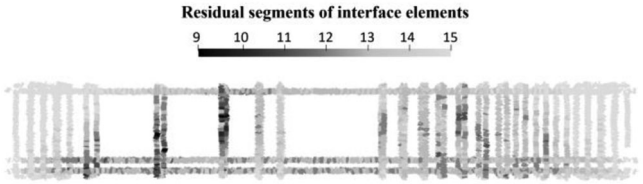

FIGURE 31 Residual segments of reinforcement-concrete interface elements at the peak load

longitudinal reinforcement (Figure 29) does not exactly follow the flexural moment diagram. This is due to shear cracking and bond-slipping of reinforcement, as shown in Figure 31, which is indicated by the broken interface elements and pull-out of the reinforcement. Although plenty of interface elements fracture, all of them do not reach their ultimate strength (the 10th segment). For the bottom reinforcement at the inner layer, the reinforcement strain at 200 mm from the support until 1030 mm is almost constant although the moment grows. It reveals the debonding of reinforcement due to longitudinal splitting cracking of the concrete, which is well-reproduced in the simulation.

Similarly, at the support, strains in bottom reinforcement (both for outer and inner reinforcement) are found not to be zero, although no flexural moment exists there, which can be attributed to the same phenomena. This is not the case for the top reinforcement, which is in the compression zone. It reveals a demand for better reinforcement anchorage in shear-critical RC members.

For the stirrup strain distribution (Figure 30), the maximum strain happens exactly at the position crossed by the critical shear crack, which is not (always) at the mid-height of the stirrup leg. Therefore, attaching a limited number of strain gauges at the mid-height of the stirrup leg, as commonly applied in concrete research, can lead to an underestimation of the contribution of stirrups to shear resistance.

6 | CONCLUSION

This research proposes a mathematical methodology to scale the constitutive parameters of the bond-slip relationships between concrete and reinforcing steel, in a beam lattice modeling framework. A simplified, generalized approach, with a limited number of input parameters, is proposed for modeling the reinforcement-concrete interaction in the random lattice model at the macro-scale. A mathematical methodology for determining the element properties of interface beam elements (strength and elastic modulus) is provided based on the stochastic analysis, considering the disorder based on the randomness of lattice

mesh and mesh size. As a result, modification factors for the strength and stiffness of interface elements are derived for both 2D and 3D analysis. Then, the proposed approach is validated at multiple levels: using two different reinforcement pull-out tests as well as flexural and shear tests of RC beams. The following are the conclusions from this study:

1. In this research, the model of pull-out failure reported in the literature was used as input and regarded as the inherent property of the reinforcement-concrete interface. Depending on boundary and confinement conditions, and with no additional input required other than concrete properties (strength and elastic modulus), both a (phenomenon of) splitting failure and the bond-slip relation for the splitting failure can be successfully predicted by the lattice model.
2. When the interface elements are not aligned with reinforcing bars, the strength and elastic modulus of interface elements should be modified by the derived factors for 2D or 3D analysis. These factors are derived considering the randomness of the lattice mesh and mesh size through a stochastic analysis.
3. The ultimate pull-out failure in one-end pull-out test of reinforcement results from the complete failure of interface elements between reinforcement and concrete, accompanied by some matrix microcracking. For simulations with non-aligned interface elements, the output bond stress-slip relationship can be well-simulated by incorporating the derived modification factors.
4. Without changing the interface input and only by changing the concrete cover thickness, as shown in the two-end reinforcement pull-out test, splitting failure and bond-slip relation of splitting failure are well-simulated with the prediction error of less than 10% in terms of ultimate bond strength. In this case, the ultimate failure is primarily due to the fracture of surrounding concrete, while interface elements still have some reserve capacity. The confinement effect of concrete cover thickness on the simulated bond-slip relation and fracture mode is well-captured without the need to change the input of interface properties.
5. Different from the regular quadratic mesh, the random triangular lattice mesh generated by Delaunay triangulation can reproduce the basic conical stress transfer mechanism in concrete, although the 3D shape of ribs on reinforcement is not explicitly modeled.
6. Using the proposed approach to simulate the interface elements in a flexure-critical RC beam, somewhat higher stiffness and smaller crack widths are observed, compared to experimental results. Still, the load-deformation behavior, crack development, failure load, and deformation capacity are well-captured, with a prediction error of 5% and 10% in terms of the peak load and maximum crack width, respectively.
7. Shear behavior of a full-scale RC beam is also well-captured with a prediction error of 10% in terms of shear strength when using the proposed approach. The numerical failure mode, load-deflection behavior, crack development, and the strain distribution along the longitudinal and transverse reinforcement show a good correlation with the experimental observations.

The proposed approach has been validated on various levels, by using various boundary conditions and without changing input parameters. It seems to be robust and does not need to be updated with fitting parameters to account for the influence of different critical factors on the bond behavior, for example, changed boundary conditions, different confinement levels of concrete, and cover thickness. The influence of these parameters is reliably predicted and obtained as a result of the model. In future, the somewhat higher stiffness of simulated structures, probably caused by modeling reinforcement-concrete interface by beam elements, can be addressed by incorporating other types of linkage elements (e.g., zero-length spring elements). Also, the current approach is limited to modeling the reinforcement that is either aligned in x or y-direction, so being aligned with the mesh direction. Although it is not expected that the angle between reinforcement and mesh direction would largely influence the results (due to irregular lattice mesh), the modeling of inclined reinforcement will be considered in future. Further research will also focus on using/extending for modeling the reinforcement-concrete bond in different types of concrete and investigating the role of shrinkage on the bond behavior.

ACKNOWLEDGMENTS

This work was supported in part by a grant from the Dutch Organization for Scientific Research (NWO) under the grant "Optimization of interface behaviour for innovative hybrid concrete structures" (Project Number: 16814), and the Key Project of the National Natural Science Foundation of China (Project Number: 52130210).

REFERENCES

Alnaggar, M., Pelessone, D., & Cusatis, G. (2019). Lattice discrete particle modelling of reinforced concrete flexural behavior. *Journal of Structural Engineering*, *145*(1), 04018231.

Avadh, K., Jiradilok, P., Bolander, J. E., & Nagai, K. (2022). 3D mesoscale simulation of the influence of corrosion on loss of tension stiffening in reinforced concrete. *Construction and Building Materials*, *339*, 127684.

Aydin, B. B., Tuncay, K., & Binici, B. (2019). Simulation of reinforced concrete member response using lattice model. *ASCE Journal of Structural Engineering*, *145*(9), 04019091.

Bado, M. F., Casas, J. R., & Kaklauskas, G. (2021). Distributed Sensing (DOFS) in Reinforced Concrete members for reinforcement strain monitoring, crack detection and bond-slip calculation. *Engineering Structures*, *226*, 111385.

Bhaduri, T., Gomaa, S., & Alnaggar, M. (2021). Coupled experimental and computational investigation of the interplay between discrete and continuous reinforcement in ultrahigh performance concrete beams. ii: mesoscale modelling. *ASCE Journal of Engineering Mechanics*, *147*(9), 04021050.

Bolander, J. E., Hong, G. S., & Yoshitake, K. (2000). Structural concrete analysis using rigid-body-spring networks. *Computer Aided Civil and Infrastructure Engineering*, *15*(2), 120–133.

Bolander, J. E., & Sukumar, N. (2005). Irregular lattice model for quasistatic crack propagation. *Physical Review B*, *71*(9), 094106.

Cai, J., Pan, J., Tan, J., & Li, X. (2020). Bond behaviours of deformed steel rebars in engineered cementitious composites (ECC) and concrete. *Construction and Building Materials*, *252*(2020), 119082.

Cervenka, V., Rimkus, A., Gribniak, V., & Cervenka, J. (2022). Simulation of the crack width in reinforced concrete beams based on concrete fracture. *Theoretical and Applied Fracture Mechanics*, *121*, 103428.

Chang, Z., Xu, Y., Chen, Y., Gan, Y., Schlangen, E., & Šavija, B. (2021). A discrete lattice model for assessment of buildability performance of 3D-printed concrete. *Computer Aided Civil and Infrastructure Engineering*, *36*(5), 638–655.

Eliáš, Jan. (2015). Generalization of load-unload and force-release sequentially linear methods. *International Journal of Damage Mechanics*, *24*(2), 279–293.

Eligehausen, R., Popov, E. P., & Bertero, V. V. (1982). Local bond stress-slip relationships of deformed bars under generalized excitations. *Proceedings of 7th European Conference on Earthquake Engineering*, Athens, Greece (pp. 69–80).

European committee for standardization (CEN). (2004). *Eurocode 2: Design of concrete structures, Part 1–1: General rules and rules for buildings*. Brussels. https://www.dica.unict.it/users/aghersi/Testi/Normativa_Europea/EN%201992-1-1a.pdf

Farooq, U., Nakamura, H., & Miura, T. (2022). Evaluation of failure mechanism in lap splices and role of stirrup confinement using 3D RBSM. *Engineering Structures*, *252*, 113570.

Farooq, U., Nakamura, H., Miura, T., & Yamamoto, Y. (2020). Proposal of bond behavior simulation model by using discretized Voronoi mesh for concrete and beam element for reinforcement. *Cement and Concrete Composites*, *110*, 103593.

Fascetti, A., Ichimaru, S., & Bolander, J. E. (2022). Stochastic lattice discrete particle modelling of fracture in pervious concrete. *Computer-Aided Civil and Infrastructure Engineering*, Advance online publication. https://doi.org/10.1111/mice.12816

Ferguson, P. M. (1966). Bond stress: The state of art report by ACI committee 408. *ACI Structural Journal*, *63*(11), 1161–1190.

Gan, Y., Rodriguez, C. R., Zhang, H., Schlangen, E., Breugel, K. V., & Šavija, B. (2021). Modelling of microstructural effects on the creep of hardened cement paste using an experimentally informed lattice model. *Computer Aided Civil and Infrastructure Engineering*, *36*, 560–576.

Gedik, Y. H., Nakamura, H., Yamamoto, Y., & Kunieda, M. (2011). Evaluation of three-dimensional effects in short deep beams using a rigid-body-spring-model. *Cement and Concrete Composites*, *33*(9), 978–991.

Goto, Y. (1971). Cracks formed in concrete around deformed tension bars. *ACI Journal*, *68*(4), 244–251.

Gribniak, V., Rimkus, A., Caldentey, A. P., & Sokolov, A. (2020). Cracking of concrete prisms reinforced with multiple bars in tension–the cover effect. *Engineering Structures*, *220*, 110979.

Gu, D., Pan, J., Mustafa, S., Huang, Y., & Luković, M. (2022). Shear transfer mechanism in reinforced engineered cementitious composite (ECC) beams: Quantification of Vs and Vc. *Engineering Structures*, *261*, 114282.

Harajli, M. H. (2009). Bond stress–slip model for steel bars in unconfined or steel, FRC, or FRP confined concrete under cyclic loading. *ASCE Journal of Structural Engineering*, *135*, 509–518.

Harajli, M. H., Hamad, B. S., & Rteil, A. A. (2004). Effect of confinement of bond strength between steel bars and concrete. *ACI Structural Journal*, *101*(5), 595–603.

Harajli, M. H., Hout, M., & Jalkh, W. (1995). Local bond stress-slip behavior of reinforcing bars embedded in plain and fiber concrete. *ACI Materials Journal*, *92*(4), 343–353.

Hordijk, D. (1993). *Local approach to fatigue of concrete*. (Doctoral dissertation), Delft University of Technology, Delft.

Iizuka, K., Higai, T., Saito, S., & Takahashi, R. (2011). Bond stress-slip-strain relationship of deformed bars including the effect of concrete cover thickness. *Journal of JSCE*, *67*, 280–296. [in Japanese].

Karam, M. S., Yamamoto, Y., Nakamura, H., & Miura, T. (2019). Mesoscale analysis for the bond behavior of concrete under active confinement using coupled RBSM and solid FEM. *Proceedings of 10th International Conference on Fracture Mechanics of Concrete and Concrete Structures (FraMCoS-X)*, Bayonne, France (pp. 1–11).

Kurumutani, M., Anzo, H., Kobayashi, K., Okazaki, S., & Hirose, S. (2017). Damage model for simulating chloride concentration in reinforced concrete with internal cracks. *Cement and Concrete Composites*, *84*, 62–73.

Lee, D. T., & Schachter, B. J. (1980). Two algorithms for constructing a Delaunay triangulation. *International Journal of Computer & Information Sciences*, *9*(3), 219–242.

Lee, S., Kang, S., Tan, K., & Yang, E. (2016). Experimental and analytical investigation on bond-slip behaviour of deformed bars embedded in engineered cementitious composites. *Construction and Building Materials*, *127*, 494–503.

Lilliu, G. (2007). *3D analysis of fracture processes in concrete*. (Doctoral dissertation), Delft University of Technology, Delft.

Luković, M., Schlangen, E., & Ye, G. (2015). Combined experimental and numerical study of fracture behaviour of cement paste at the microlevel. *Cement and Concrete Research*, *73*, 123–135.

Luković, M., Yang, Y., Schlangen, E., & Hordijk, D. (2017). On the potential of lattice type model for predicting shear capacity of reinforced concrete and SHCC structures. *Proceedings of fib Symposium 2017*, Maastricht, the Netherlands, (pp. 804–813).

Mirza, S. M., & Houde, J. (1979). Study of bond stress-slip relationships in reinforced concrete. *ACI Structural Journal*, *76*(2), 19–46.

Mustafa, S., Singh, S., Hordijk, D., Schlangen, E., & Luković, M. (2022). Experimental and numerical investigation on the role of interface for crack-width control of hybrid SHCC concrete beams. *Engineering Structures*, *251*, 113378.

Oliver-Leblond, C. (2013). *Comportement à rupture des structures: Description à deux échelles des mécanismes locaux appliquée aux matériaux fragiles renforcés*. École normale supérieure de Cachan.

Pan, Y., Prado, A., Porras, R., Hafez, O. M., & Bolander, J. E. (2017). Lattice modelling of early-age behavior of structural concrete. *Materials*, *10*(3), 231.

Qian, Z. (2012). *Multiscale modelling of fracture processes in cementitious materials*. (Doctoral dissertation), Delft University of Technology, Delft.

Regan, P. E., & Kennedy Reid, I. L. (2004). Shear strength of RC beams with defective stirrup anchorages. *Magazine of Concrete Research*, *56*(3), 159–166.

Rimkus, A., Cervenka, V., Gribniak, V., & Cervenka, J. (2020). Uncertainty of the smeared crack model applied to RC beams. *Engineering Fracture Mechanics*, *233*, 107088.

Sasano, H., Maruyama, I., Nakamura, A., Yamamoto, Y., & Teshigawara, M. (2018). Impact of drying on structural performance of reinforced concrete shear walls. *Journal of Advanced Concrete Technology*, *16*(5), 210–232.

Šavija, B., Luković, M., Pacheco, J., & Schlangen, E. (2013). Cracking of the concrete cover due to reinforcement corrosion: A two-dimensional lattice model study. *Construction and Building Materials*, *44*, 626–638.

Schlangen, E., & Garboczi, E. J. (1997). Fracture simulations of concrete using lattice models: computational aspects. *Engineering Fracture Mechanics*, *57*(2), 319–332.

Ye, Z., Zhang, W., & Gu, X. (2018). Deterioration of shear behavior of corroded reinforced concrete beams. *Engineering Structures*, *168*, 708–720.

Yip, M., Mohle, J., & Bolander, J. E. (2005). Automated modelling of three-dimensional structural components using irregular lattices. *Computer Aided Civil and Infrastructure Engineering*, *20*, 393–407.

How to cite this article: Gu, D., Mustafa, S., Pan, J., & Luković, M. (2022). Reinforcement-concrete bond in discrete modeling of structural concrete. *Computer-Aided Civil and Infrastructure Engineering*, 1–22. https://doi.org/10.1111/mice.12937